The evolution of star formation activity in galaxy groups

G. Erfanianfar, P. Popesso, A. Finoguenov, S. Wuyts, D. Wilman, A. Biviano, F. Ziparo, M. Salvato, K. Nandra, D. Lutz, et al.

▶ **To cite this version:**

G. Erfanianfar, P. Popesso, A. Finoguenov, S. Wuyts, D. Wilman, et al.. The evolution of star formation activity in galaxy groups. Monthly Notices of the Royal Astronomical Society, 2014, 445 (3), pp.2725–2745. 10.1093/mnras/stu1883 . hal-01441033

HAL Id: hal-01441033
https://hal.science/hal-01441033

Submitted on 18 Dec 2021

HAL is a multi-disciplinary open access archive for the deposit and dissemination of scientific research documents, whether they are published or not. The documents may come from teaching and research institutions in France or abroad, or from public or private research centers.

L'archive ouverte pluridisciplinaire **HAL**, est destinée au dépôt et à la diffusion de documents scientifiques de niveau recherche, publiés ou non, émanant des établissements d'enseignement et de recherche français ou étrangers, des laboratoires publics ou privés.

Distributed under a Creative Commons Attribution 4.0 International License

Monthly Notices
of the
ROYAL ASTRONOMICAL SOCIETY

MNRAS **445,** 2725–2745 (2014) doi:10.1093/mnras/stu1883

The evolution of star formation activity in galaxy groups

G. Erfanianfar,[1,2]★ P. Popesso,[1,2] A. Finoguenov,[3] S. Wuyts,[2] D. Wilman,[2] A. Biviano,[4] F. Ziparo,[5] M. Salvato,[2] K. Nandra,[2] D. Lutz,[2] D. Elbaz,[6] M. Dickinson,[7] M. Tanaka,[8] M. Mirkazemi,[2] M. L. Balogh,[9,10] M. B. Altieri,[11] H. Aussel,[6] F. Bauer,[12,13] S. Berta,[2] R. M. Bielby,[14] N. Brandt,[15] N. Cappelluti,[16] A. Cimatti,[17] M. Cooper,[18] D. Fadda,[19] O. Ilbert,[20] E. Le Floch,[6] B. Magnelli,[21] J. S. Mulchaey,[22] R. Nordon,[23] J. A. Newman,[24] A. Poglitsch[2] and F. Pozzi[17]

Affiliations are listed at the end of the paper

Accepted 2014 September 9. Received 2014 September 9; in original form 2013 December 17

ABSTRACT

We study the evolution of the total star formation (SF) activity, total stellar mass (ΣM_*) and halo occupation distribution (HOD) in massive haloes by using one of the largest X-ray selected sample of galaxy groups with secure spectroscopic identification in the major blank field surveys (ECDFS, CDFN, COSMOS, AEGIS). We provide an accurate measurement of star formation rate (SFR) for the bulk of the star-forming galaxies using very deep mid-infrared *Spitzer* MIPS and far-infrared *Herschel* PACS observations. For undetected IR sources, we provide a well-calibrated SFR from spectral energy distribution (SED) fitting. We observe a clear evolution in the level of SF activity in galaxy groups. The total SF activity in the high-redshift groups ($0.5 < z < 1.1$) is higher with respect to the low-redshift ($0.15 < z < 0.5$) sample at any mass by 0.8 ± 0.12 dex. A milder difference (0.35 ± 0.1 dex) is observed between the low-redshift bin and the groups at $z \sim 0$. We show that the level of SF activity is declining more rapidly in the more massive haloes than in the more common lower mass haloes. We do not observe any evolution in the HOD and total stellar mass–halo mass relations in groups. The picture emerging from our findings suggests that the galaxy population in the most massive systems is evolving faster than galaxies in lower mass haloes, consistently with a 'halo downsizing' scenario.

Key words: catalogues – galaxies: evolution – cosmology: observations – large-scale structure of Universe – infrared: galaxies.

1 INTRODUCTION

One of the most fundamental correlations between the properties of galaxies in the local Universe is the so-called morphology–density relation (Davis & Geller 1976; Dressler 1980). A plethora of studies utilizing multiwavelength tracers of activity have shown that late-type star-forming galaxies favour low-density regimes in the local Universe (e.g. Lewis et al. 2002; Gómez et al. 2003; Hogg et al. 2004; Blanton et al. 2005). In particular, the cores of massive galaxy clusters are full of massive spheroids that are dominated by old stellar populations. A variety of physical processes might be effective in suppressing star formation (SF) and affecting the morphology of cluster and group galaxies. Two big families of such processes can be identified: (i) interactions with other cluster members and/or with the cluster potential and (ii) interactions with the hot gas that permeates massive galaxy systems. In the current standard paradigm for structure formation, dark matter collapses into haloes in a bottom-up fashion: small objects form first and subsequently merge into progressively larger systems. In this context, galaxy groups are the building blocks of galaxy clusters. Galaxy groups have at any epoch a volume density orders of magnitude higher than those of massive clusters, which represents the rare and extreme specimen at the high-mass end of the dark halo mass function (Jenkins et al. 2001). This is confirmed by the observational evidence that groups are the most common environment of galaxies in the present-day Universe, containing 50–70 per cent of the galaxy population (Geller & Huchra 1983; Eke et al. 2005). This naturally implies that processes taking place in the group environment can have a significant impact on the evolution of the galaxy population as a whole.

The main debate now centres on the role of galaxy 'internal' versus 'external' processes as driving mechanisms of the galaxy evolution, or, according to an old-fashion approach, the 'nature' versus 'nurture' scenario. In the current paradigm of galaxy

★ E-mail: erfanian@mpe.mpg.de

© 2014 The Authors
Published by Oxford University Press on behalf of the Royal Astronomical Society

Downloaded from https://academic.oup.com/mnras/article/445/3/2725/1041622 by guest on 18 December 2021

formation, the 'internal' processes are mainly linked to the co-evolution of the host galaxy and its central black hole (Di Matteo, Springel & Hernquist 2005; Croton et al. 2006; De Lucia et al. 2006; Hopkins et al. 2006). However, as pointed out by De Lucia et al. (2012), the nature versus nurture dichotomy is an ill-posed problem. In the current paradigm of galaxy formation, these physical internal and external processes are coupled with a history bias that is an integral part of the hierarchical structure formation of cosmic structure (Cooper et al. 2010; De Lucia et al. 2012). Wilman et al. (2013) have demonstrated that haloes in overdense regions statistically form earlier and merge more rapidly than haloes in regions of lower density (Gao et al. 2004). This differential evolution leaves a trace on the observable properties of galaxies that inhabit different regions at any cosmic epoch (De Lucia et al. 2012). This aspect makes the interpretation of the pieces of observational evidence even more difficult. In fact, binning galaxies according to their stellar mass does not suffice to disentangle the role of nature and nurture. For instance, two galaxies of identical mass at some cosmic epoch can end up having different stellar masses if one of them falls on to a cluster and the other remains in a region of average density. An important attempt to investigate from the observational point of view the inter-relationships between stellar mass, star formation rate (SFR) and environment comes from Peng et al. (2010) in the Sloan Digital Sky Survey (SDSS) and zCOSMOS surveys. This study shows that (a) two distinct processes, mass (internal) quenching and environment (external) quenching, are both operating since $z \sim 1$, (b) environment quenching occurs as large-scale structure develops and is more effective on satellite galaxies, (c) mass quenching is more efficient for central and generally more massive galaxies. The limit of this analysis is mainly in the definition of the environment that relies on the local galaxy density, which is only a poor proxy of the DM halo mass.

In the last decade, a lot of effort has been devoted to the study of high-redshift groups to investigate the possibility of a differential evolution of group galaxies with respect to field galaxies. A big step forward was made thanks to the advent of very deep multiwavelength surveys conducted on several blank fields, such as the Great Observatories Origin Deep Survey-South and -North (GOODS-S and GOODS-N, respectively), the Extended *Chandra Deep Field*-South (ECDFS), the Cosmological Evolution Survey (COSMOS) and the All-wavelength Extended Groth strip International Survey (AEGIS). Those surveys combine deep photometric (from the X-rays to the far-infrared wavelengths) and spectroscopic (down to $i_{\rm AB} \sim 24$ mag and $b \sim 25$ mag) observations over relatively large areas to lead, for the first time, to the construction of statistically significant samples of groups up to high redshift ($z \sim 1.3$–1.6; e.g. Finoguenov et al. 2010 and Bielby et al. 2010). In this context, the main outcome of these surveys is that group galaxies show a much faster evolution with respect to the field galaxies. For instance, the formation of the galaxy red sequence, which leads to the local dichotomy between red and blue galaxies, happens earlier in groups than in the field especially at high stellar masses (Cooper et al. 2007; Wilman et al. 2009; Iovino et al. 2010; Kovač et al. 2010; Wilman & Erwin 2012). It seems also that group galaxies undergo a substantial morphological transformation. Indeed, groups at $z \sim 1$ host a transient population of 'red spirals' which is not observed in the field (Jeltema et al. 2007; Tran et al. 2008; Balogh et al. 2009; Wolf et al. 2009; Mei et al. 2012).

Most analyses so far have concentrated on comparisons of the star-forming properties of the group galaxy population as a whole with those of field galaxies. However, it is also important to assess the dependence (if any) of the star-forming properties of group galaxies on their system global properties, such as the mass, velocity dispersion and X-ray luminosity of the groups at different epochs to understand if and how the evolution of the SF activity depends on these variables. A way of looking at the evolution of the SF activity in galaxy systems is to consider global quantities such as the total SFR, which is the sum of the SFRs of all the galaxies in a system (see e.g. Popesso et al. 2007) or the fraction of star-forming galaxies in a system (see e.g. Poggianti et al. 2006). Understanding how the relation between these global quantities and the group properties changes with time can teach us how the evolution of galaxies depends on the environment where they live. For this purpose, we create the largest homogeneously X-ray selected sample of groups at $0.15 < z < 1$ by using the deepest available X-ray surveys conducted with *Chandra* and *XMM–Newton* on the ECDFS, CDFN, COSMOS and Extended Groth Strip (EGS) regions. In addition, we use the latest and deepest available *Spitzer* MIPS and *Herschel* PACS (Photoconducting Array Camera and Spectrometer; Poglitsch et al. 2010) mid- and far-infrared surveys, respectively, conducted on the same blank fields to retrieve an accurate measure of the SFR of individual group galaxies. This is the first of a series of papers analysing the relation between SF activity and galaxy environment defined as the membership of a galaxy to a massive dark matter halo. In this paper, we carefully describe the catalogue and present a calibration of all the relevant quantities involved in our analysis. We use this unprecedented data set to study the evolution of the relation between the total SFR in galaxy groups at $0.15 < z < 1$ with the group global properties, mainly the total halo mass, and the stellar mass content of the groups and halo occupation distribution (HOD) to understand how the group galaxy population evolves though cosmic times.

The paper is organized as follows. In Section 2, we describe our data set. In Section 3, we describe how all relevant quantities are estimated. In Section 4, we describe our results and in Section 5 we discuss them and draw our conclusions. We adopt a Chabrier (2003) initial mass function (IMF), $H_0 = 71$ km s^{-1} Mpc^{-1}, $\Omega_{\rm m} = 0.3$, $\Omega_\Lambda = 0.7$ throughout this paper.

2 THE DATA SET

The aim of this work is to analyse the evolution of the SF activity in galaxy groups. For this purpose, we build a data set which combines wide-area surveys with good X-ray coverage, deep photometry and high spectroscopic coverage. Galaxy clusters and groups are permeated by a hot intracluster medium radiating optically diffuse thermal emission in the X-ray band. Under the condition of hydrostatic equilibrium, the gas temperature and density are directly related to halo mass. A tight relation (rms 0.15 dex) exists also between the cluster dynamical mass and the X-ray luminosity ($L_{\rm X}$; Pratt et al. 2007; Rykoff et al. 2008). A similar scaling relation, though with a larger scatter, holds also in the galaxy group mass regime (Sun 2012, rms 0.3 dex). Thus, the X-ray selection is the best way to select galaxy groups and clusters and to avoid incorrect galaxy group identifications due to projection effects associated with optical selection techniques. In addition, deep and accurate multiwavelength catalogues are necessary in order to identify the group membership and to study the properties of the group galaxy population. Thus, we combine X-ray selected group catalogues and photometric and spectroscopic galaxy catalogues of four major blank field surveys: AEGIS field, COSMOS, the ECDFS and the CDFN. Throughout our analysis, we use spectroscopic redshifts to define the group membership and the multiwavelength photometric information for studying the galaxy properties. For calibration purposes, we will

Downloaded from https://academic.oup.com/mnras/article/445/3/2725/1041622 by guest on 18 December 2021

also make use of photometric redshifts. In the following section, we describe the multiwavelength data set of each field.

2.1 The blank fields

2.1.1 AEGIS

The AEGIS brings together deep imaging data from X-ray to radio wavelengths and optical spectroscopy over a large area (0.5–1 deg^2; Davis et al. 2007). This survey includes *Chandra*/ACIS X-ray (0.5–10 keV; Laird et al. 2009), *Galaxy Evolution Explorer* (*GALEX*) ultraviolet (1200–2500 Å), Canada–France–Hawaii Telescope (CFHT)/MegaCam Legacy Survey optical (3600–9000 Å), CFHT/CFH12K optical (4500–9000 Å; Coil et al. 2004), *Hubble Space Telescope* (*HST*)/ACS optical (4400–8500 Å; Lotz et al. 2008), Palomar/WIRC near-infrared (NIR; 1.2–2.2 μm; Bundy et al. 2006), *Spitzer*/IRAC mid-infrared (3.6, 4.5, 5.8, 8 μm; Barmby et al. 2008), *Herschel* far-infrared (100, 160 μm), Very Large Array (VLA) radio continuum (6–20 cm; Willner et al. 2012) and a large spectroscopic data set.

In particular, the X-ray data come from sensitive *Chandra* and *XMM–Newton* observations of this field which lead to one of the largest X-ray selected samples of galaxy groups catalogue to date (Erfanianfar et al. 2013). The total X-ray exposure time with *Chandra* in this field is about 3.4 Ms with a nominal exposure of 800 ks in three central fields. The *XMM–Newton* observations in the southern part of this field have an exposure of 100 ks. The spectroscopic information is taken from different spectroscopic surveys performed in this field. The AEGIS field, as part of the EGS field, has been targeted with the DEEP2 galaxy redshift survey (Davis et al. 2003; Newman et al. 2013) and it is the only field that has been a subject of extensive spectroscopic follow-up data in DEEP3 (Cooper et al. 2011, 2012). In the DEEP2 fields, EGS is the only field which is not colour selected, so it gives us a nearly complete sample with redshift. In addition to DEEP2 and DEEP3, EGS is located in SDSS coverage so we have additional spectra for low-redshift galaxies. We also used redshifts of spectroscopic galaxies obtained in follow-up observations of the DEEP2 sample with the Hectospec spectrograph on the Multiple Mirror Telescope (MMT; Coil et al. 2009).

Furthermore, the EGS field is located at the centre of the third wide field of the Canada–France–Hawaii Telescope Legacy Survey (CFHTLS-Wide3, W3) which is imaged in u^*, g', r', i' and z' filters down to $i' = 24.5$ with photometric data for 366 190 galaxies (Brimioulle et al. 2008). The EGS field also contains the CFHTLS D3 field, which covers 1 deg^2 with *ugriz* imaging to depths ranging from 25.0 in z to 27 in g. For this work, we have used the T0006 release[1] of the CHTLS Deep data. The CFHTLS Deep field also contains NIR coverage in the *JHK* bands via the WIRCam Deep Survey (Bielby et al. 2012). This covers 0.4 deg^2 of the D3 field and provides deep imaging to ∼24.5 (AB) in the three NIR bands. Photometric redshifts in the region covered by the NIR data were determined using the LE PHARE code as described in Bielby et al. (2012).

2.1.2 COSMOS

The Cosmological Evolution Survey (COSMOS) is the largest survey ever made using the *HST*. With its 2 deg^2 of coverage, COSMOS enables the sampling of the large-scale structure of the Universe and reduces cosmic variance (Scoville et al. 2007). In particular, COSMOS guarantees full spectral coverage, with X-ray (*Chandra* and *XMM–Newton*), UV (*GALEX*), optical (Subaru), NIR (CFHT), mid-infrared (*Spitzer*), *Herschel* far-infrared (100, 160 μm), sub-millimetric (MAMBO) and radio (VLA) imaging. Furthermore, the X-ray information provided by the 1.5 Ms exposure with *XMM–Newton* (53 pointings on the whole field, 50 ks each; Hasinger et al. 2007) and the additional 1.8 Ms exposure with *Chandra* in the central square degree (Elvis et al. 2009) enable robust detections of galaxy groups out to $z \sim 1.2$ (Finoguenov et al. 2007; George et al. 2011, 2013).

COSMOS has been targeted by many spectroscopic programmes at different telescopes and has a broad spectral coverage. The spectroscopic follow-up is still continuing and so far includes the zCOSMOS survey at VLT/VIMOS (Lilly et al. 2007, 2009), Galaxy Environment Evolution Collaboration 2 (GEEC2) survey with the GMOS spectrograph on the Gemini telescope (Balogh et al. 2011; Mok et al. 2013), Magellan/IMACS (Trump et al. 2007) and MMT (Prescott et al. 2006) campaigns, observations at Keck/DEIMOS (PIs: Scoville, Capak, Salvato, Sanders, Kartaltepe) and FLWO/FAST (Wright, Drake & Civano 2010).

The COSMOS photometric catalogue (Capak et al. 2007; Capak 2009) contains multiwavelength photometric information for $\sim 2 \times 10^6$ galaxies over the entire field. The position of galaxies has been extracted from the deep i-band imaging (Taniguchi et al. 2007). A limit of 80 per cent completeness is achieved at $i_{AB} = 26.5$. The optical catalogue of Capak et al. (2007) and Capak (2009) includes 31 bands (2 bands from the GALEX, 6 broad bands from the SuprimeCam/Subaru camera, 2 broad bands from MEGACAM at CFHT, 14 medium and narrow bands from SuprimeCam/Subaru, J band from the WFCAM/UKIRT camera, H and K bands from the WIRCAM/CFHT camera, and the 4 IRAC/*Spitzer* channels). In particular, We take the catalogue provided by Ilbert et al. (2009, 2010). They cross-match the S-COSMOS Sanders et al. (2007) 3.6 μm selected catalogue with the multiwavelength catalogue (Capak et al. 2007; Capak 2009) and calculate photo-z, stellar masses and SFR in a consistent way by using the LE PHARE code (Ilbert et al. 2009, 2010).

2.1.3 ECDFS

ECDFS is observed broadly from X-ray to radio wavelengths and centred on one of the most well-studied extragalactic fields in the sky (e.g. Giavalisco et al. 2004; Rix et al. 2004; Lehmer et al. 2005; Quadri et al. 2007; Miller et al. 2008; Padovani et al. 2009; Cardamone et al. 2010; Damen et al. 2011; Xue et al. 2011). The smaller *Chandra Deep Field*-South (CDFS, $\alpha = 03^h32^m25^s$, $\delta = -27^\circ49'58''$), in the central part of ECDFS, is currently the deepest X-ray survey with *Chandra* (4 Ms) and *XMM–Newton* (3 Ms) programmes.

The redshift assemblage in the ECDFS and the smaller CDFS and GOODS-S regions is achieved by complementing the spectroscopic redshifts contained in the Cardamone et al. (2010) catalogue with all new publicly available spectroscopic redshifts, such as the one of Silverman et al. (2010) and the Arizona CDFS Environment Survey (Cooper et al. 2012). We clean the new catalogue of redshift duplications for the same source by matching the Cardamone et al. (2010) catalogue with the Cooper et al. (2012) and the Silverman et al. (2010) catalogue within 1 arcsec and by keeping the most accurate z_{spec} entry (smaller error and/or higher quality flag) in case of multiple entries (see Ziparo et al. 2013 for a more detailed

[1] http://terapix.iap.fr/cplt/T0006-doc.pdf

Downloaded from https://academic.oup.com/mnras/article/445/3/2725/1041622 by guest on 18 December 2021

discussion). We also include the very high quality redshifts of the GMASS survey (Cimatti et al. 2008) using the same procedure. The total number of secure redshifts in the sample is 5080 out of 7277 total, unique targets.

We use the multiwavelength photometric data from the catalogue of Cardamone et al. (2010). It includes a total of 10 ground-based broad bands (U, $U38$, B, V, R, I, z, J, H, K), 4 IRAC bands (3.6, 4.5, 5.8, 8.0 μm), and 18 medium-band imaging (*IA*427, *IA*445, *IA*464, *IA*484, *IA*505, *IA*527, *IA*550, *IA*574, *IA*598, *IA*624, *IA*651, *IA*679, *IA*709, *IA*738, *IA*767, *IA*797, *IA*856). The catalogue includes multiwavelength SEDs and photometric redshifts for ∼80 000 galaxies down to $R_{\rm AB} \sim 27$.

2.1.4 CDFN

The *Chandra Deep Field*-North (CDFN) survey is one of the deepest 0.5–8.0 keV surveys ever made. The *Chandra* survey is comprised of two partially overlapping ∼1 Ms ACIS-I exposures covering a total of 448 arcmin^2, of which ≈160 arcmin^2 has 1.7–1.9 Ms of exposure. In addition, there is 150 ks of good *XMM–Newton* exposure. The GOODS-N field is within the CDFN centres at RA $=12^{\rm h}36^{\rm m}55^{\rm s}$, Dec. $=+62^\circ14'15''$ (J2000) and has become one of the most well-studied extragalactic fields in the sky with existing observations among the deepest at a broad range of wavelengths (e.g., Alexander et al. 2003; Morrison et al. 2010; Cooper et al. 2011; Elbaz et al. 2011). GOODS-N covers an area of approximately 10 arcmin × 16 arcmin (Giavalisco et al. 2004).

We use the multiwavelength catalogue of GOODS-N built by Berta et al. (2010), who adopted the Grazian et al. (2006) approach for the point spread function (PSF) matching. The catalogue includes ACS *bviz* (Giavalisco et al. 2004), Flamingos *JHK* and *Spitzer* IRAC data. Moreover, MIPS 24 μm (Magnelli et al. 2009) and deep U, *Ks* (Barger, Cowie & Wang 2008) have been added. The catalogue is also complemented by the spectroscopic redshift compilation of Barger et al. (2008).

2.2 X-ray analysis

All the blank fields considered in our analysis are observed extensively in the X-ray with *Chandra* and *XMM–Newton*. First, we remove point sources in both of the *Chandra* and *XMM–Newton* images following the procedure explained in Finoguenov et al. (2009). Then the residual images were co-added, taking into account the different sensitivity of each instrument. The 'residual' image, free of point sources, is then used to identify extended emission. Groups and clusters are selected as extended emission with at least 4σ significance with respect to the background (see Finoguenov et al. 2009 for further details regarding the precise definition of background and detection significance level). A redshift to each system on the basis of spectroscopic redshifts, when available, or otherwise photometric redshift is assigned. The X-ray luminosity $L_{\rm X}$ and r_{500} are determined iteratively, based on the aperture flux and recalculating the correction for the missing flux. M_{200} is determined via the scaling relation from weak lensing by the final $L_{\rm X}$ and so is r_{200}. The r_{200} is the radius at which the density of a cluster is equal to 200 times the critical density of the Universe ($\rho_{\rm c}$) and is defined as $M_{200} = (4\pi/3)200\rho_{\rm c}r_{200}^3$. After taking into account the possible missed flux through the use of the beta model, the total masses M_{200}, within r_{200}, are estimated based on the measured $L_{\rm X}$ and its errors, using the scaling relation from weak lensing calibration of Leauthaud et al. (2010). The intrinsic scatter for mass in this relation is 20 per cent (Leauthaud et al. 2010; Allevato et al. 2012) which is larger than a formal statistical error associated with the measurement of L_X.

The X-ray group catalogues derived with this approach comprise 52 detections in AEGIS (Erfanianfar et al. 2013), 277 detections in the COSMOS field (George et al. 2011), 50 detections in the ECDFS (Finoguenov et al., in preparation) and 27 detection in CDFN. We present the full CDFN X-ray group catalogue in Appendix A. In the following section, we describe how we select a subsample of 'secure' groups and how we associate them with the respective galaxy population.

2.2.1 Group identification

To associate the respective galaxy population with any X-ray extended emission and to define properly the group redshift, we follow the same procedure described in Erfanianfar et al. (2013) and performed on the AEGIS X-ray data set. We extend here this procedure to all the other fields described in the previous section. In brief, we estimate the galaxy overdensity along the line of sight in the region of each X-ray extended emission following the red sequence technique (Finn et al. 2010). Additionally, we screen for the existence of an overdensity of red galaxies in the third dimension using the spectroscopic redshift distribution of the X-ray extended source.

As described in Erfanianfar et al. (2013), we assigned to each X-ray extended source a flag that describes the quality of the identification. We define the following flags:

(1) flag=1 indicates a confident redshift assignment, significant X-ray emission and a well-determined centre of red galaxies with respect to X-ray emission centre;

(2) flag=2 indicates that the centring has a large uncertainty (∼15 arcsec);

(3) flag=3 indicates no secure spectroscopic confirmation but good centring; and

(4) flag=4 or more depending on the survey indicates that we have uncertain redshifts due to the lack of spectroscopic objects and red galaxies, and also a large uncertainty in centring or unreliable cases for which we could not identify any redshift.

For the purpose of this work, we consider only X-ray extended emission with a secure redshift definition with flag 1 or 2. Out of the initial 406 X-ray group candidates in the four considered fields, we identify 244 secure groups. The secure redshift estimate is used to refine the initial X-ray luminosity of the groups and, thus, the mass M_{200} with the scaling relation of Leauthaud et al. (2010) as described in the previous paragraph. The final step of the analysis is the identification of the group galaxy members via dynamical analysis as described below.

2.2.2 Group membership

In order to properly define the galaxy membership of each group, we identify among our 244 secure groups those which are relatively isolated. Indeed, the presence of a close companion may bias the estimate of the velocity dispersion of the group and, thus, also the galaxy membership definition which relies on this quantity. This procedure leads to a subsample of 211 clean isolated groups. We follow the procedure described in Erfanianfar et al. (2013) to estimate the group velocity dispersion and the galaxy membership definition. The procedure is iterative and it needs a first guess of the velocity dispersion to define the redshift interval around the group redshift to determine the initial galaxy membership. We derive the first guess

Downloaded from https://academic.oup.com/mnras/article/445/3/2725/1041622 by guest on 18 December 2021

of the velocity dispersion from the group's X-ray luminosity L_X by using the relation of Leauthaud et al. (2010). This velocity dispersion provides the intrinsic velocity dispersion [$\sigma(v)_{\rm intr}$, which can be achieved by subtracting the errors of the redshift measurements in quadrature from the rest-frame velocity dispersion] of the group. We estimate, then, the observed velocity dispersion by considering the redshift of the group ($z_{\rm group}$) and the errors of the redshift in our spectroscopic samples, $\langle\Delta(v)\rangle^2$, according to these relations:

$$\sigma(v)^2_{\rm rest} = \sigma(v)^2_{\rm intr} + \langle\Delta(v)\rangle^2 \quad (1)$$

$$\sigma(v)_{\rm obs} = \sigma(v)_{\rm rest} \times (1 + z_{\rm group}). \quad (2)$$

We consider as initial group members all galaxies within $|z - z_{\rm group}| < \delta(z)_{\rm max}$, where $\delta(z)_{\rm max} = 2\frac{\sigma(v)_{\rm obs}}{c}$ and within virial radii (r_{200}) from the X-ray centre. We recompute the observed velocity dispersion of the groups, $\sigma(v)_{\rm obs}$, using the 'gapper' estimator method which gives more accurate measurements of velocity dispersion for small-size groups (Beers, Flynn & Gebhardt 1990; Wilman et al. 2005) in comparison to the usual formula for standard deviation (see Erfanianfar et al. 2013 for more details). The observed velocity dispersion is estimated according to

$$\sigma(v)_{\rm obs} = 1.135c \times \frac{\sqrt{\pi}}{N(N-1)} \sum_{i=1}^{n-1} \omega_i g_i, \quad (3)$$

where $w_i = i(N - i)$, $g_i = z_{i+1} - z_i$ and N is the total number of spectroscopic members. In this way, we measure the velocity dispersion using the line-of-sight velocity gaps where the velocities have been sorted into ascending order. The factor 1.135 corrects for the 2σ clipping of the Gaussian velocity distribution. We iterate the entire process until we obtain a stable membership solution. We then calculate errors for our velocity dispersions using the Jackknife technique (Efron 1982). The procedure can be considered reliable for groups with at least 10 galaxy members. The 10 galaxy members' threshold is reached for 36 groups out of 211. For the groups with less than 10 members but still more than 5 members within r_{200}, we base the velocity dispersion estimate on M_{200} and the relation between σ and r_{200} as in Carlberg, Yee & Ellingson (1997). This leads to a sample of 111 groups out of 211. Fig. 1 shows the L_X–σ relation for X-ray groups with more than 10 spectroscopic members, where σ is estimated via dynamical analysis. The solid red line shows the power-law fit to the relation. The bisector procedure is used for this fit (Akritas & Bershady 1996). We also plot the L_X–σ relation (dashed blue line) expected from scaling relations obtained for a sample of groups with similar luminosities in the $0 < z < 1$ redshift range in COSMOS (Leauthaud et al. 2010). The consistency between two relations ensures that the estimate of the velocity dispersion derived from the X-ray luminosity and the one calculated via dynamical analysis are in good agreement.

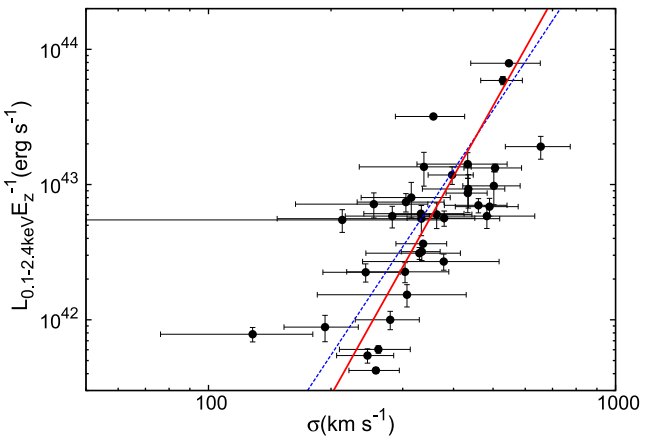

Figure 1. L_X–σ relation for X-ray groups. The dashed blue line shows our expectation for the L_X–σ relation from scaling relations (Leauthaud et al. 2010) and the solid red line is our bisector fit to data.

Once we have the estimate of the velocity dispersion of each group, we define as group members all galaxies within $2 \times r_{200}$ in the angular direction and $\pm 3 \times (\sigma/c) \times (1 + z_{\rm group})$ in the line-of-sight direction in order to consider also the infalling regions of the groups. When a member galaxy is associated with more than one group, we consider it as a member of the group for which the distance to the galaxy is lowest in units of virial radii.

2.3 Infrared data

For all considered fields, we use the deepest available *Spitzer* MIPS 24 μm and PACS 100 and 160 μm data sets. For COSMOS, these are coming from the public *Spitzer* 24 μm (Sanders et al. 2007; Le Floc'h et al. 2009) and PEP PACS 100 and 160 μm data (Lutz et al. 2011). Both *Spitzer* MIPS 24 μm and PEP source catalogues are obtained by extracting sources using NIR priors as described in Magnelli et al. (2009). In short, IRAC and MIPS 24 μm source positions are used to detect and extract MIPS and PACS sources, respectively, at 24, 100 and 160 μm. This is feasible since extremely deep IRAC and MIPS 24 μm observations are available for the COSMOS field (Scoville et al. 2007). The source extraction is based on a PSF-fitting technique, presented in detail in Magnelli et al. (2009). The association between 24 μm and PACS sources with their optical counterparts, taken from the optical catalogue of Capak et al. (2007), is done via a maximum likelihood method (see Lutz et al. 2011, for details).

The same approach is used also for the AEGIS field, where we use the *Spitzer* MIPS 24 and PEP PACS 100 and 160 μm catalogues produced by the PEP team (see Magnelli et al. 2009).

In the CDFS and GOODS regions, the deepest available MIR and FIR data are provided by the *Spitzer* MIPS 24 μm Fidel Programme (Magnelli et al. 2009) and by the combination of the PACS PEP (Lutz et al. 2011) and GOODS-*Herschel* (Elbaz et al. 2011) surveys at 70, 100 and 160 μm. The GOODS-*Herschel* survey covers a smaller central portion of the entire GOODS-S and GOODS-N regions. Recently, the PEP and the GOODS-H teams combined the two sets of PACS observations to obtain the deepest ever available PACS maps (Magnelli et al. 2013) of both fields. The ECDFS area has been observed in the PEP survey as well, yet having a higher flux limit. As for the COSMOS catalogues, the 24 μm and PACS sources are associated with their optical counterparts via a maximum likelihood method (see Lutz et al. 2011, for details).

For all galaxies identified as galaxy group members, we use the MIPS and PACS data to accurately estimate the IR bolometric luminosity and, thus, the SFR. We compute the IR luminosities integrating the spectral energy distribution (SED) templates from Elbaz et al. (2011) in the range 8–1000 μm. The PACS (70, 100 and 160 μm) fluxes, when available, together with the 24 μm fluxes are used to find the best-fitting templates among the main-sequence (MS) and starburst (Elbaz et al. 2011) templates. When only the 24 μm flux is available for undetected PACS sources, we rely only on this single point and we use the MS template for extrapolating the $L_{\rm IR}$. Indeed, Ziparo et al. (2013) show that the MS template turns out to be the best-fitting template in the majority of the cases with common PACS and 24 μm detection. Ziparo et al. (2013) show also that by using only 24 μm

Downloaded from https://academic.oup.com/mnras/article/445/3/2725/1041622 by guest on 18 December 2021

data and the MS template, there could be a slight underestimation (10 per cent) only above $z \sim 1.7$ or $L_{\rm IR}^{24} > 10^{11.7}\,{\rm L}_{\odot}$. In larger fields such as COSMOS and ECDFS, there is a larger probability to find rare strong star-forming off-sequence galaxies at $L_{\rm IR}^{24} > 10^{11.7}\,{\rm L}_{\odot}$ even at low redshift. However, those sources should be captured by the *Herschel* observations given the very high luminosity threshold. Thus, it would not be a problem in getting a proper estimate of the $L_{\rm IR}$ from the best-fitting templates also for these rare cases. The SFR for these sources is then estimated via the Kennicutt (1998) relation and then corrected from Salpeter IMF to Chabrier IMF for consistency with $\rm SFR_{SED}$ and stellar mass.

2.3.1 Stellar masses and SFR from SED fitting

Due to the flux limits of the MIPS and PACS catalogues in the four considered blank fields, the IR catalogues are sampling only the MS region and cannot provide an SFR estimate for galaxies below the MS or in the region of quiescence. For a complete census of the SF activity of the group galaxies, we need, however, an estimate of the SFR of all group members. For this reason, we complement the SFR estimates derived from IR data ($\rm SFR_{IR}$), as described in the previous section, with an alternative estimate of the SFR. SFRs based either on the SED fitting technique ($\rm SFR_{SED}$) or on rest-frame UV observations ($\rm SFR_{UV}$) are both reliable candidates. According to Ziparo et al. (2013), the scatter of the $\rm SFR_{UV}$–SFR_{IR} relation is always bigger (at every redshift) with respect to the $\rm SFR_{SED}$–$\rm SFR_{IR}$ calibration. So, we use $\rm SFR_{SED}$ as an alternative estimate of the SFR. Thus, for all galaxies undetected in MIPS and PACS maps, we use the $\rm SFR_{SED}$ taken from the following catalogues:

(1) in AEGIS, SFR estimated with FAST (Kriek et al. 2009) taken from Wuyts et al. (2011);
(2) in COSMOS, SFR estimated with LE PHARE taken from Ilbert et al. (2010);
(3) in ECDFS, SFR estimated with LE PHARE, from Ziparo et al. (2013);
(4) in CDFN, SFR estimated with FAST (Kriek et al. 2009) taken from Wuyts et al. (2011).

The same catalogues provide also an estimate of the galaxy stellar mass. All $\rm SFR_{SED}$ and stellar mass estimates are in Chabrier IMF.

Ziparo et al. (2013) point out that, in general, the stellar masses and $\rm SFR_{SED}$ derived from Wuyts et al. (2011), Ilbert et al. (2010) and Ziparo et al. (2013) are all in agreement when compared on a common galaxy subsample. According to Ziparo et al. (2013), the scatter around the one-to-one relation is of the order of 0.6 dex. Indeed, previous studies (Papovich, Dickinson & Ferguson 2001; Shapley et al. 2001, 2005; Santini et al. 2009) already demonstrate that, while stellar masses are rather well determined (within a factor of 2) by very different methods, the SED fitting procedure does not strongly constrain SF histories at high redshifts, where the uncertainties become larger due to the SFR–age–metallicity degeneracies. This degeneracy leads to the confusion of young, obscured star-forming galaxies with more massive, old, more quiescent galaxies. Wuyts et al. (2011) confirm that the $\rm SFR_{SED}$ provides a quite good estimate of the SFR for moderately star-forming galaxies and fails to provide a good estimate for very obscured objects.

Indeed, if we examine the scatter of the $\rm SFR_{SED}$–$\rm SFR_{IR}$ relation, we clearly see a degeneracy with the stellar mass, as shown in the left-hand panels of Fig. 2. This degeneracy is stronger than the one due to the redshift, as shown in Wuyts et al. (2011), though the two aspects are related via selection effects (only massive star-forming galaxies generally have spectroscopic redshifts at high redshift). The mass dependence of the scatter is different from field to field and depends on the method used for the SED fitting. This is probably due to two aspects. First, any blank field is characterized by a different data set in terms of multiwavelength coverage (number and type of broad-band filters) and, thus, by a different sampling of the galaxy SED. Secondly, different recipes, thus different SF histories, and different fitting techniques are used for estimating the stellar masses and the $\rm SFR_{SED}$. This also explains why there is such a large scatter in the $\rm SFR_{SED}$ derived with different methods.

The result of this exercise shows that we cannot use the $\rm SFR_{SED}$–$\rm SFR_{IR}$ relation observed in one of the fields to calibrate the $\rm SFR_{SED}$ of the other fields or obtained with a different method. Thus, we use the following approach. In order to correct a posteriori for the stellar mass bias in the $\rm SFR_{SED}$, we fit the plane $\rm SFR_{IR}$–$\rm SFR_{SED}$–mass, separately for each field. The best-fitting relation is listed below for AEGIS and CDFN (same fitting procedure):

$$\rm SFR_{IR} = -6.16 + 0.59 \times SFR_{SED} + 0.66 \times \mathit{M}_{*}, \quad (4)$$

for COSMOS:

$$\rm SFR_{IR} = -4.54 + 0.61 \times SFR_{SED} + 0.49 \times \mathit{M}_{*}, \quad (5)$$

and for ECDFS and GOODS-S:

$$\rm SFR_{IR} = -4.56 + 0.63 \times SFR_{SED} + 0.49 \times \mathit{M}_{*}. \quad (6)$$

Once this calibration is used to correct the $\rm SFR_{SED}$ with the additional information of the stellar mass, the scatter around the $\rm SFR_{SED}$–$\rm SFR_{IR}$ relation decreases to 0.21, 0.23 and 0.12 dex in comparison to $\rm SFR_{IR}$ for galaxies with more than $10^{10}\,{\rm M}_{\odot}$ in AEGIS, COSMOS and ECDFS, respectively, as shown in the central panels of Fig. 2. The values of the scatter are still 0.34, 0.42 and 0.44 in AEGIS, COSMOS and ECDFS, respectively, when the whole mass range is considered.

We adopt this calibration to correct a posteriori the $\rm SFR_{SED}$ estimates for all IR undetected galaxies above $\log({\rm SFR}) > -0.5$. We think that this calibration is applicable in the SFR range considered here to IR undetected galaxies for the following reasons. Elbaz et al. (2011) show that the IR SEDs of star-forming galaxies are not evolving with redshift and that, instead, there is a much stronger dependence on the location of galaxies with respect to the galaxy MS. In addition, Buat et al. (2009), by using *Spitzer* MIPS data, also show that the dust attenuation expressed in terms of $\log(L_{\rm IR}/L_{\rm UV})$ as a function of the $\log(L_{\rm IR} + L_{\rm UV})$, which is proportional to the SFR, seems to be redshift independent (fig. 2 of Buat et al. 2009) in particular between redshift 0 and 1 as considered in this work. The same work also shows that $\log(L_{\rm IR}/L_{\rm UV})$ as a function of the rest-frame K-band (L_K) luminosity, which is a proxy for the stellar mass, does not show any redshift dependence. This was recently confirmed also by Berta et al. (2013) with the most recent *Herschel* PEP and Herschel Multi-tiered Extragalactic Survey (HerMES) data. Thus, the substantial lack of evolution of IR and rest-frame UV properties of galaxies of a given mass and SFR would suggest that the low-redshift IR detected galaxies that populate the low SF regime of Fig. 2 can be used to calibrate the $\rm SFR_{SED}$ of IR undetected galaxies in the same SFR regime at higher redshift.

We point out that in the COSMOS field, as shown in the central panels of Fig. 2, our calibration does not consistently move all galaxies to the one-to-one line (middle panel). Highly star-forming galaxies still show a slightly too low $\rm SFR_{SED}$ with respect to the IR measure. This is probably due to the fact that in the case of the Ilbert et al. (2010) SED fitting results, a plane in log–log space is not the best analytical form and, thus, it does not provide the best

Downloaded from https://academic.oup.com/mnras/article/445/3/2725/1041622 by guest on 18 December 2021

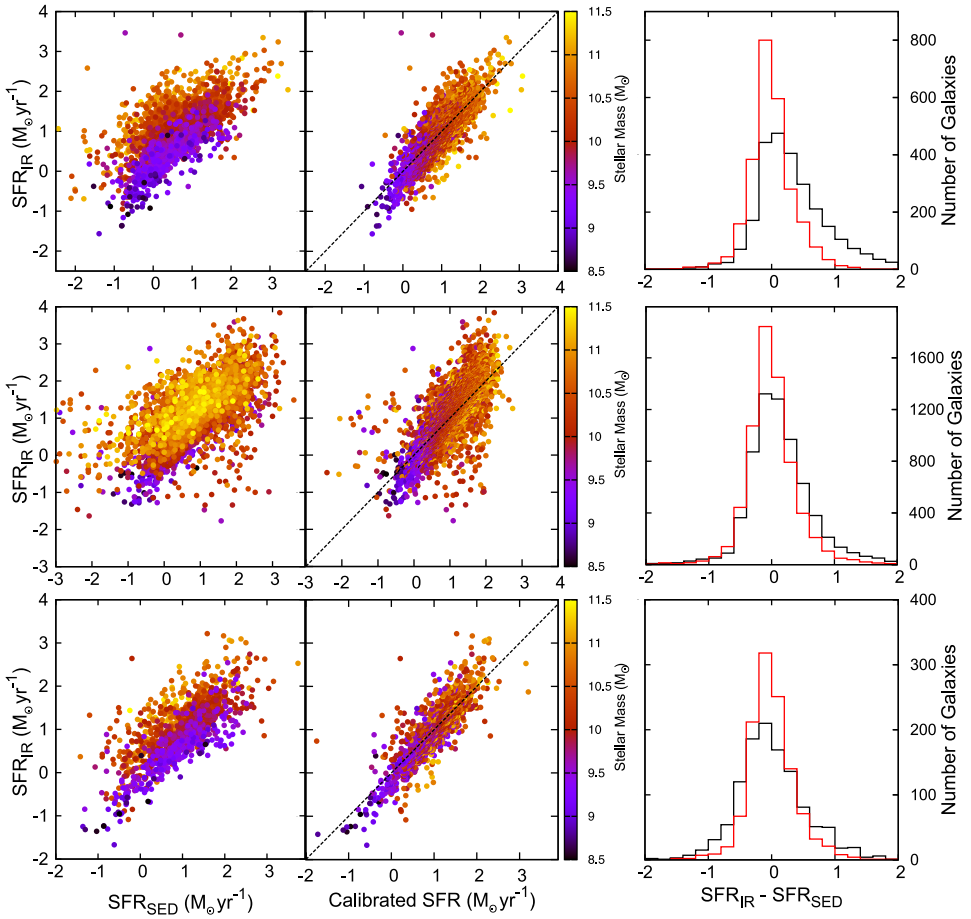

Figure 2. The left-hand panels show SFR_{IR} versus SFR_{SED} colour-coded by stellar mass before re-calibration for EGS, COSMOS and GOODS-S from top to bottom, respectively. The middle panels show corresponding SFR_{IR} versus re-calibrated SFR_{SED}. The dashed line shows the one-to-one relation. The right-hand panels show the histogram of corresponding SFR_{IR}–SFR_{SED}. The black and red histograms show before (black) and after (red) re-calibration.

representation of the SFR_{IR}–SFR_{SED}–mass relation. However, we still improve the agreement within SFR_{SED} and SFR_{IR} by more than a factor of 2 even in this field.

2.4 The final galaxy group and group galaxy samples

The aim of our analysis is to study how the SF activity in group-sized haloes depends on the global properties of the systems. In order to do that, we would need to sample the complete group galaxy population in stellar mass and SFR. However, since the group members are spectroscopically selected, we need to consider how the spectroscopic selection function drives our galaxy selection and, thus, how it can affect our results. We point out that we cannot define a galaxy sample which is, at the same time, complete in stellar mass and SFR. For this purpose, we check how the spectroscopic completeness in the IRAC band translates into a completeness in mass and SFR. For ECDFS and CFDN, this is already done in Ziparo et al. (2013). For the new data sets of AEGIS and COSMOS, we follow the same approach of the mentioned work. This is done separately in two redshift bins ($0.15 < z < 0.5$ and $0.5 < z < 1.1$). The reference catalogues used to estimate this completeness are the photometric catalogues described in Section 2.3.1. All those photometric catalogues are IRAC selected at 3.6 or 4.5 μm and should ensure photometric completeness down to at least $m_{AB}(3.6\,\mu m) \sim 23$. From these catalogues, we extract, for each field, the photometric redshift, the stellar mass and the SFR information derived from the SED fitting technique, after replacing the SFR_{SED} with SFR_{IR}, where available, and after correcting SFR_{SED} with the calibration presented in Section 2.3.1. Given the high accuracy of the photometric redshifts of Cardamone et al. (2010), Wuyts et al. (2011) and Ilbert et al. (2010), we assume the photometric redshifts, and the physical properties based on those, to be correct. We, then, estimate the completeness per stellar mass and SFR bins, respectively, as the ratio between the number of galaxies with spectroscopic redshift and the total number of galaxies in that bin. This procedure allows us to determine how the spectroscopic selection, based on the photometric information (e.g. colour, magnitude cuts, etc.), affects the choice of galaxies as spectroscopic targets according to their physical properties. Indeed, Fig. 3 illustrates while in any bin of stellar mass, the most star-forming galaxies are preferentially selected, the most massive galaxies are preferentially observed at any given SFR.

Thus, we follow the following approach to deal with spectroscopic incompleteness. We fix the stellar mass threshold to a value of 10^{10} $M_{\odot}$, which guarantees a minimum spectroscopic completeness (40 per cent) for our analysis. We impose that this minimum completeness level (40 per cent) above the stellar mass threshold (10^{10} $M_{\odot}$) must be reached in the region of the group. This completeness is estimated as follows. We consider a cylinder along the line of sight of the group with a radius of $2 \times r_{200}$ from the X-ray centre and half-width in redshift equal to $5 \times \sigma_{\Delta z/(1+z)}$, where

Downloaded from https://academic.oup.com/mnras/article/445/3/2725/1041622 by guest on 18 December 2021

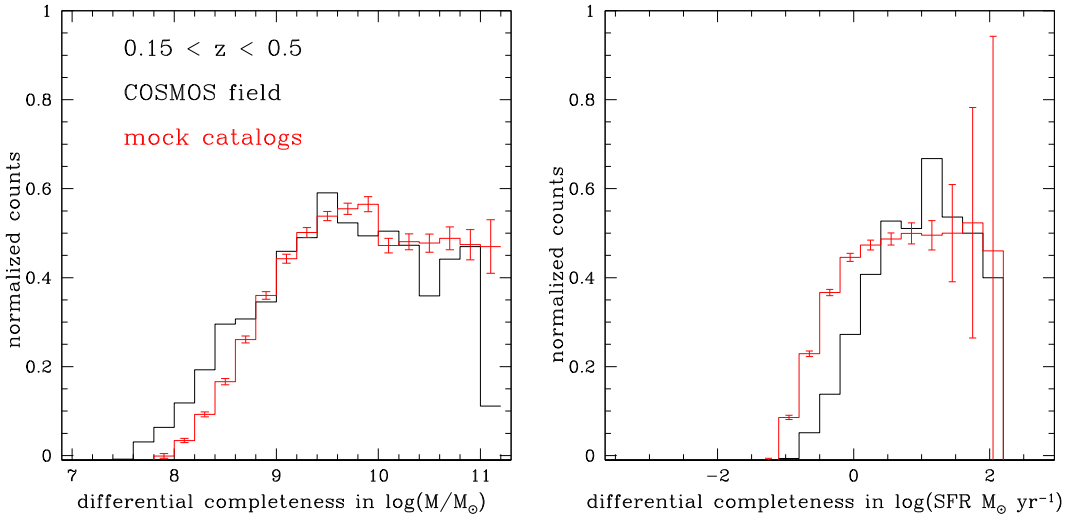

Figure 3. Left-hand panel: spectroscopic completeness per stellar mass bin in the low-redshift sample (black histogram) and in the simulated 'incomplete' mock catalogue (red line) in the same redshift range. Right-hand panel: spectroscopic completeness per SFR bin for the low-redshift sample (black histogram) and in the simulated 'incomplete' mock catalogue (red line).

$\sigma_{\Delta z/(1+z)}$ is the error of the photometric redshifts in each survey. This width is set to be much larger than the photometric redshift uncertainty and still small enough to sample the group region. The completeness is the ratio of the number of galaxies with spectroscopic redshift to the number of galaxies with spectroscopic or photometric redshift within this cylinder, with stellar mass above the given mass threshold. We perform the same analysis with different values of the cylinder half-width (up to $10\times\ \sigma_{\Delta z/(1+z)}$) and we obtain consistent measures of the completeness in mass. This minimum completeness level of 40 per cent is fulfilled for almost all groups in the AEGIS, ECDFS and CDFN due to a very high and spatially homogeneous spectroscopic completeness. However, the 40 per cent threshold is hardly reached in many of the COSMOS group regions. The requirements are mainly fulfilled by the groups in the zCOSMOS region and by the GEEC2 groups. To deal with the reliability of our method, we analyse the possible biases induced by the spectroscopic selection function using mock catalogues. Our approach is explained in Section 3.

We point out that the use of the full zCOSMOS and the GEEC2 spectroscopic sample increases the level of completeness in the COSMOS field by 20 per cent in the mean and in the group regions with respect to Ziparo et al. (2013).

The final group sample is shown in Fig. 4. The sample comprises 83 galaxy groups in the redshift range $0.15 < z < 1.1$. In order to study the evolution of the relation between the SF activity in groups and the system global properties, we divide the sample into two subsamples at $0.15 < z < 0.5$ (31 galaxy groups) and $z > 0.5$ (52 galaxy groups). For 29 of 83 galaxy groups, we have velocity dispersion from dynamical analysis and for the rest of them from X-ray properties. 50 of galaxy groups have Flag=1 and the remaining 33 have Flag=2.

2.5 The reference nearby group sample

Our group sample does not cover the local Universe. Indeed, we apply a cut at $z = 0.15$ in order to sample the same cosmic time epoch in the two redshift bins (∼3 Gyr) considered in our analysis. In order to follow the evolution of the group galaxy population down to $z \sim 0$, we complement our sample with a reference sample of nearby

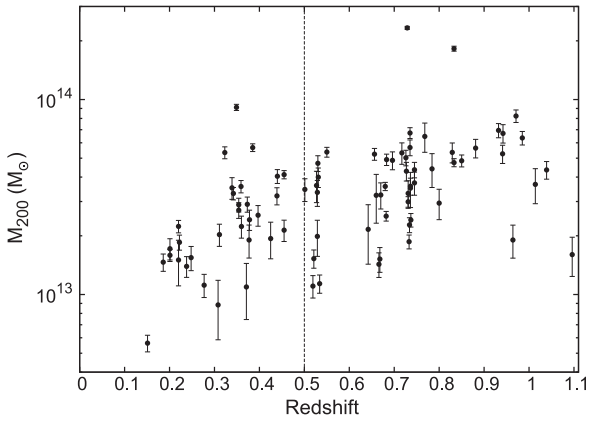

Figure 4. M_{200} versus redshift for the final sample of galaxy groups in our analysis. The vertical dashed line separates low-z and high-z sample.

groups. Unfortunately, an X-ray selected sample of nearby groups in the same mass range as our sample with the same information as our groups does not exist. Most of the X-ray selected samples available in the literature have a quite complicated selection function. In addition, we need also a complete, spectroscopically confirmed, membership of any system and auxiliary information of the group galaxy stellar mass and SF activity. Thus, we choose as a reference sample an optically selected sample of nearby groups drawn from the SDSS and with a well-studied and clean selection function. The group catalogue and its general properties are discussed in Yang et al. (2007). The catalogue is drawn from the clean New York University Value-Added Galaxy Catalog (NYU-VAGC) DR4 galaxy catalogue (Blanton et al. 2005), which is a subsample of the SDSS DR4 galaxy spectroscopic catalogue. The group selection is based on the halo-based group finder of Yang et al. (2005), which is optimized for grouping galaxies that reside in the same dark matter halo. The performance of this group finder is extensively tested using mock galaxy redshift surveys constructed from the conditional luminosity function model (van den Bosch, Yang & Mo 2003; Yang, Mo & van den Bosch 2003; Yang et al. 2004). The Yang et al. (2007) group catalogue provides for each system the group membership and an estimate of the halo mass (M_{200}; see Yang et al. 2007 for

Downloaded from https://academic.oup.com/mnras/article/445/3/2725/1041622 by guest on 18 December 2021

a detailed discussion). In order to study the SF activity of nearby groups, we complement the group galaxy catalogue of Yang et al. (2007) with the stellar masses and the SFR based on SDSS Hα emission estimated by Brinchmann et al. (2004). These quantities are corrected from aperture to total and to the same IMF used in our work. We also apply the same stellar mass cut ($M_* > 10^{10}$) and completeness level (>40 per cent) in the nearby group sample for consistency.

2.6 The Millennium mock catalogues

In order to estimate the errors involved in our analysis and check for possible biases due to the spectroscopic incompleteness, we follow the same approach as used in Ziparo et al. (2013) based on the mock catalogues provided by the Millennium Simulation (Springel et al. 2005). The Millennium Simulation follows the hierarchical growth of dark matter structures from redshift $z = 127$ to the present (Springel et al. 2005). Out of several mock catalogues created from the Millennium Simulation, we choose to use those of Kitzbichler & White (2007) based on the semi-analytical model of De Lucia et al. (2006). The simulation assumes the concordance Λ cold dark matter cosmology and follows the trajectories of $21\,603^3 \sim 1.0078 \times 10^{10}$ particles in a periodic box 500 Mpc h^{-1} on a side. Kitzbichler & White (2007) make mock observations of the artificial universe by positioning a virtual observer at $z \sim 0$ and finding the galaxies which lie on a backward light cone. The backward light cone is defined as the set of all light-like worldlines intersecting the position of the observer at redshift zero. We select as information from each catalogue the Johnson photometric band magnitudes available (R_J, I_J and K_J), the redshift, the stellar mass and the SFR of each galaxy with a cut at $I_J < 26$ to limit the data volume to the galaxy population of interest. In order to simulate the spectroscopic selection function of the surveys used in this work, we choose one of the available photometric bands (R_J) and extract randomly in each magnitude bin a percentage of galaxies consistent with the percentage of systems with spectroscopic redshift in the same magnitude bin observed in each of our surveys. We do this separately for each survey, since each field shows a different spectroscopic selection function as shown in Fig. 5. We follow this procedure to extract randomly 25 catalogues for each survey from different light cones. The 'incomplete' mock catalogues, produced in this way, tend to reproduce, to a level that we consider sufficient to our needs, the selection of massive and highly star-forming galaxies observed in the real galaxy samples, as already shown in Ziparo et al. (2013).

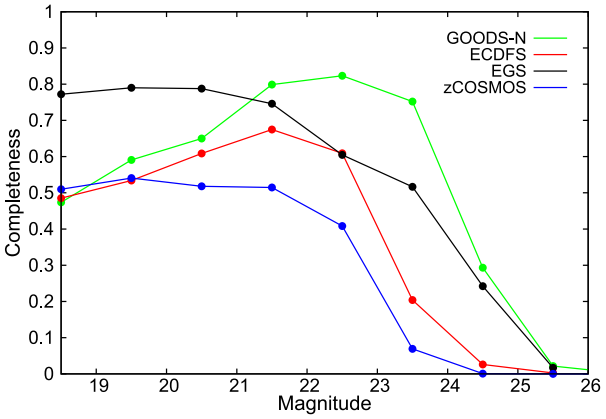

Figure 5. Spectroscopic completeness for different fields in *R*-band magnitude. We use *v*-band magnitude for GOODS-N.

We note that the galaxy mock catalogues of the Millennium Simulation fail in reproducing the correct distribution of star-forming galaxies in the SFR–stellar mass plane, as already shown in Elbaz et al. (2007) at higher redshift ($z \sim 1$), although they provide a rather good representation of the local Universe. This is caused by the difficulty of the semi-analytical models of predicting the observed evolution of the galaxy stellar mass function and the cosmic SF history of our Universe (Kitzbichler & White 2007; Guo et al. 2010). We stress here that this does not produce a problem for our approach. Indeed, we aim to understand the bias induced by selection function like the spectroscopic selection function of our data set by using the Millennium galaxy mock catalogues. In other words, we only need to extract mock catalogues randomly to reproduce the same bias in selecting, on average, the same percentage of most star-forming and most massive galaxies of the parent sample. By comparing the results obtained in the biased randomly extracted mock catalogues and the unbiased parent catalogue, we estimate the bias of our analysis. Since in both biased and unbiased mock catalogues the underestimation of the SFR or the stellar mass of high-redshift galaxies exists, it does not affect the result of this comparative analysis. We also stress that the aim of this analysis is only to provide a way to interpret our results in terms of possible biases introduced by the spectroscopic selection function and not to provide correction factors for our observational results.

3 ESTIMATE OF TOTAL M_*, TOTAL SFR AND HOD OF GALAXY GROUPS

In this section, we describe our method for estimating the total stellar mass (ΣM_*), the total star formation rate (ΣSFR) and the HOD of the galaxy groups in our sample. As explained in Section 2.4, we impose a stellar mass cut at $M_* > 10^{10}$ M$_\odot$ since below this limit the spectroscopic completeness is rather low in all considered fields (see the left-hand panel of Fig. 3). The HOD of each group, $N(M_* > 10^{10}\,\mathrm{M}_\odot)$, is defined by the number of galaxies with stellar mass above $M_* > 10^{10}$ M$_\odot$. The total stellar mass and SFR of each system are estimated as the sum of the group galaxy members stellar mass and SFR, respectively, with mass above the given limit. We correct for spectroscopic incompleteness by dividing ΣM_*, ΣSFR and $N(M_* > 10^{10}\,\mathrm{M}_\odot)$ by the spectroscopic completeness estimated as explained in Section 2.4. In order to check if there are biases in our estimates due to the spectroscopic selection function or to our method, and to calculate the uncertainties of each quantity, we use the galaxy mock catalogues described in Section 2.6. For this purpose, we extract from the original Kitzbichler & White (2007) mock catalogue a sample of galaxy groups in the same mass and redshift range of the observed sample. We base our selection on the dark matter halo virial mass which, according to De Lucia et al. (2006), is consistent with the mass calculated within r_{200}, as in the observed group sample. The members of the groups are identified by the same Friends-of-Friends (FoF) identification number, defined according to the FoF algorithm described in De Lucia et al. (2006). We assume that the group galaxy members identified by the FoF algorithm, which takes into account also the real 3D spatial distribution of galaxies, are the correct ('true') group members. The 'true' velocity dispersion, ΣSFR, ΣM_* and N are, thus, the one based on this membership.

We apply, then, our method for calculating the membership, the velocity dispersion, total M_*, total SFR and HOD on the 'incomplete' mock catalogues described in Section 2.6, which also include the effect of the different spectroscopic selection functions. For each group, we assume the coordinates of the central galaxy (the

Downloaded from https://academic.oup.com/mnras/article/445/3/2725/1041622 by guest on 18 December 2021

identification of central and satellite galaxies is provided in the mock catalogue) as group centre coordinates. These estimates are based on the 2D projected galaxy distribution and redshift information as in the real data set. In this way, we take into account both projection and incompleteness effects. These quantities provide the 'observed' velocity dispersion, ΣSFR, ΣM_* and N.

3.1 Reliability of group membership and velocity dispersion estimate

In order to check if our method is able to recover efficiently the membership of each group, we compare the completeness and the contamination of the membership obtained in our analysis with the original group membership identified by the FoF algorithm of the mock catalogue. The completeness is estimated by computing the fraction of 'true' members identified by our method. The contamination is estimated by calculating the fraction of interlopers (galaxy identified as group members by our method but not in the original mock catalogue). Fig. 6 shows the completeness level (top panel) and the contamination level (bottom panel) of our group membership. The dashed histograms in both panels show the completeness and contamination levels obtained if we considered all members without any stellar mass cut. The completeness level is quite high (>90 per cent), but on average 35 per cent of the members are interlopers. If we apply a mass cut of $10^{10}\,M_{\odot}$, the completeness level reaches almost in all cases 100 per cent with a much lower contamination fraction (solid histograms). It is clear that our method is much more robust in identifying rather massive galaxy members, which are likely more clustered in the phase space, than low-mass galaxies. The red and blue histograms (Fig. 7) indicate the cases in which the velocity dispersion first guess is estimated

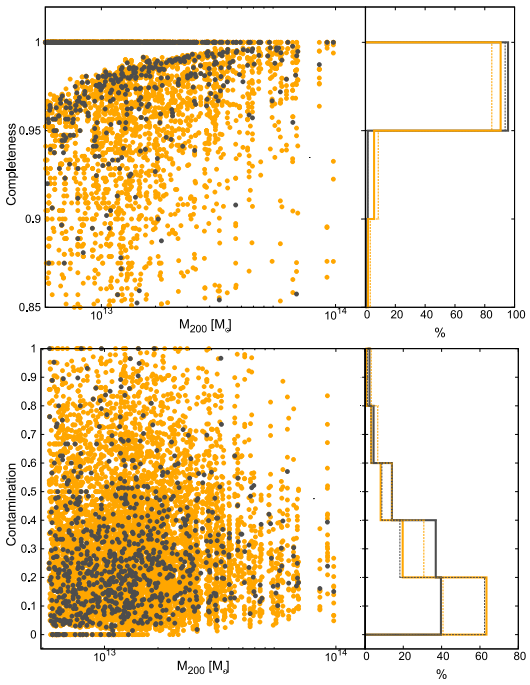

Figure 6. Completeness and contamination level of the member galaxies using the gapper estimator method with initial condition from M_{200} (grey points) and M_{200} with error (orange points) in the mock catalogue. The right-hand panels show corresponding histograms. The solid lines in the histograms show galaxies with $M_* > 10^{10}\,M_{\odot}$ and the dashed histograms are related to the whole sample.

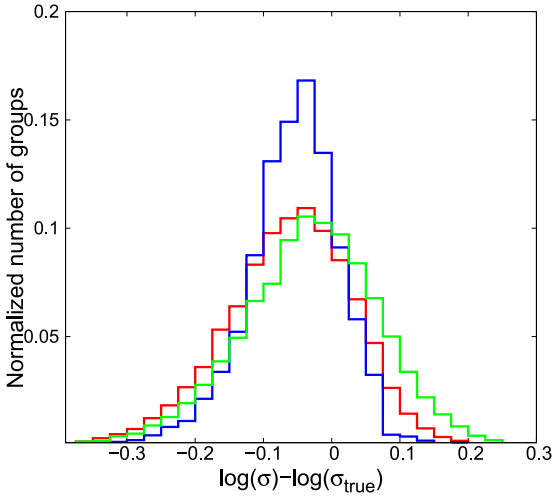

Figure 7. Distribution of the residuals of the logarithm of the 'true' and 'observed' velocity dispersion. The blue histogram shows the distribution of the residuals obtained from the original mock catalogues. The red histogram shows the distribution obtained if we take into account the error on M_{200} derived from L_X as done in the real data set. The green histogram shows the same diagram but with the 'observed' velocity dispersion estimated on the basis of the 'incomplete' mock catalogue.

from the mock catalogue M_{200} without and with error, respectively (see below). After performing the same recovery test on the 'incomplete' mock catalogue, we check that the completeness level is driven by the mean simulated completeness of the sample, while the contamination level remains at the same values.

We estimate the 'observed' velocity dispersion on the basis of this membership to take into account the effect of spectroscopic incompleteness. We measure the 'observed' σ as in the real data set. In other words, we base the velocity dispersion estimate on M_{200} and the relation between σ and r_{200} as in Carlberg et al. (1997) for groups with less than 10 members and on the dynamical analysis for groups with more than 10 galaxies. We consider also that our first guess for the velocity dispersion is affected by the uncertainty in the M_{200} in the observed data set, which is retrieved via L_X–M_{200} correlation. To take this into account, we add a random error to the M_{200} of the group provided by the mock catalogue. The scatter of the L_X–M_{200} relation is quoted about 20 per cent in the group mass regime based on the estimation via stacking analysis (Leauthaud et al. 2010; Allevato et al. 2012). However, to be conservative, we use the L_X–T_X relation and scatter reported in Sun et al. (2011) to estimate a scatter in the L_X–M_{200} relation. We use a value of 0.3 dex in our exercise. The green histogram of Fig. 7 shows the residual distribution between the 'true' and 'observed' velocity dispersion. The two values are in rather good agreement with a scatter of 0.1 dex. The main source of scatter is given by the spectroscopic incompleteness. Indeed, if we perform the same test by using the original 'complete' mock catalogue, the scatter decreases to 0.06 dex (blue histogram) and it is due to projection effects. The uncertainty in the first guess of the velocity dispersion does not affect significantly the final estimate. Indeed, without including this source of error, the scatter decreases only to 0.09 dex (red histogram).

As shown in Fig. 7, the peak of the residual distribution is not zero but it shows that we tend to underestimate the true velocity dispersion by ∼20 per cent. This shows that the Carlberg et al. (1997) relation (used for estimating the first guess, in general, and the velocity dispersion for systems with less than 10 members, in

Downloaded from https://academic.oup.com/mnras/article/445/3/2725/1041622 by guest on 18 December 2021

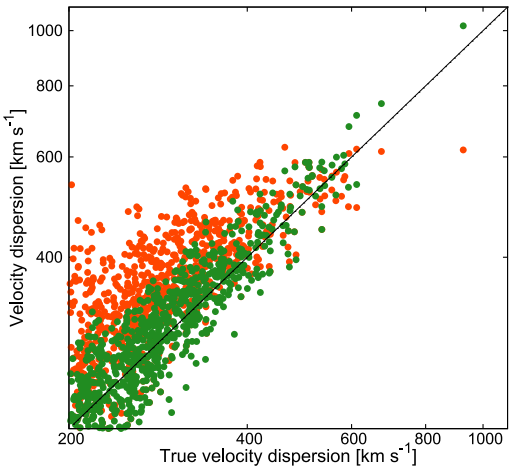

Figure 8. Velocity dispersion from gapper estimator versus true velocity dispersion for mock groups. The orange points show the choice of constant initial velocity dispersion and the green one is based on the initial velocity dispersion computed from M_{200}.

particular) is not itself a source of scatter but it could cause a bias in the estimation of velocity dispersion.

We also point out that using the estimate of M_{200} for deriving the velocity dispersion first guess is a fundamental ingredient of our analysis. Indeed, if we use a constant value for the first guess, as usually done in the literature, we find that the scatter in the relation between 'true' and 'observed' velocity dispersion increased significantly as shown in Fig. 8 (orange points) and there is no good correlation between the two quantities.

3.2 Reliability of total M_*, total SFR and HOD

As for the 'observed' velocity dispersion, we also estimate the 'observed' total stellar mass, total SFR and HOD by applying our method to the 'incomplete' mock catalogues to include the effect of projection and spectroscopic incompleteness. Each estimate is obtained after applying our stellar mass cut at $M_* > 10^{10}\,\mathrm{M}_\odot$. We also apply the correction for incompleteness as described in Section 2.4. Fig. 9 shows the comparison of the 'true' and 'observed' quantities. We find rather good agreement between the two values in all cases. However, we notice a large scatter (0.3 dex) between the 'true' and 'observed' total SFR and a smaller scatter for 'true' versus 'observed' total M_* (0.17 dex) and HOD (0.15 dex). This different behaviour of the scatter is due to two aspects. On average, the galaxies contaminating the group membership are field galaxies, likely less massive, due to mass segregation (less massive galaxies prefer low-density regions while more massive galaxies are mostly located in high-density environments; Scodeggio et al. 2009), and more star-forming than group galaxies. This is true in particular for the Millennium Simulation mock catalogues that are affected by an overabundance of red and dead galaxies in groups due to the satellite overquenching problem described in Weinmann et al. (2009). The result of this overquenching is that the level of the SF in group galaxies is suppressed with respect to less crowded environments. Thus, in the case of groups with a low number of galaxies, the presence of even one contaminant with a high SFR can highly alter the total level of SF activity. On the other hand, group galaxies tend to be rather massive and the addition of one or few field galaxies of average mass does not affect much the total M_* of the system. Thus, the uncertainty turns out to be much larger in the total SFR than in the total M_* or the HOD. Since in the local Universe we do not observe such a high abundance of red and dead satellite in groups as in the mocks (Weinmann et al. 2009), it is likely that the uncertainty from the total SFR estimated in the Millennium Simulation mock catalogues is overestimating the actual uncertainty.

The low level contamination (see previous section) also explains why in some cases we observed a slightly larger number of galaxies in groups with respect to the 'true' value.

4 RESULTS

In this section, we analyse several relations. First, we study the correlation between the total SFR in groups versus the group global properties such as L_X, σ_v and M_{200}. Since L_X and σ_v are the only independent measurements and they also exhibit a relation with a tight scatter (Fig. 1), we discuss in particular only the Σ(SFR)–M_{200} relation to relate the evolution of the SF activity of the group population to the total DM halo mass. However, all the relations derived are listed in Table 1. As previously mentioned, we divide our sample into two 'low' and 'high' redshift bins ($0.15 < z < 0.5$ and $0.5 < z < 1.1$). The two redshift bins are defined in order to have enough statistics and to sample a comparable fraction of the age of the Universe (∼3 Gyr) at different epochs. However, we must take into account that the two bins are rather wide and a significant evolution in terms of stellar population can occur in galaxies in such a large amount of time.

In the low-redshift bin, a Spearman test confirms that in none of the considered cases there is a significant correlation, while there is a rather poor correlation between the total mass M_{200} and the group redshift as already visible in Fig. 4. Thus, at least in the low-redshift bin, the different evolutionary state of the galaxy population of groups can be an additional source of scatter in the analysed relations but it does not affect the slope of the relation.

However, at high redshift we observe a quite significant correlation between each quantity and the redshift. These correlations are induced by the strong correlation between M_{200} and the group redshift as visible in Fig. 4 at $z > 0.5$. This correlation is due to the X-ray selection that tends to select higher mass systems at high redshift. In order to take this selection effect into account, we select a subsample of the high-redshift groups in the redshift range $0.5 < z < 0.8$. This subsample comprises 38 systems and it does not show any correlation between M_{200}, Σ(SFR) or M_* or HOD with the group redshift. We use this subsample to check whether the observed correlations between the aforementioned quantities and their slopes are driven by a redshift dependence.

We perform the analysis of each correlation by estimating the quantities within r_{200} and $2 \times r_{200}$. The results obtained within r_{200} are consistent with the corresponding results in $2 \times r_{200}$. We present in this section the results obtained within $2 \times r_{200}$ since this is the case with the best statistics.

4.1 ΣSFR, ΣM_* versus M_{200} and HOD

The upper panel of Fig. 10 shows the ΣSFR–M_{200} relation in the low- (blue points) and high-redshift (red points) bins. A Spearman correlation test shows a much more significant positive correlation in the high-z sample and a very mild correlation in the low-z one (see Table 1).

We first investigate the possibility that the lack of a significant correlation in the low-redshift bin could be due to the low number statistics. Indeed, the low-redshift bin contains 31 galaxy groups. This relatively low number together with the scatter due to the differences in

Downloaded from https://academic.oup.com/mnras/article/445/3/2725/1041622 by guest on 18 December 2021

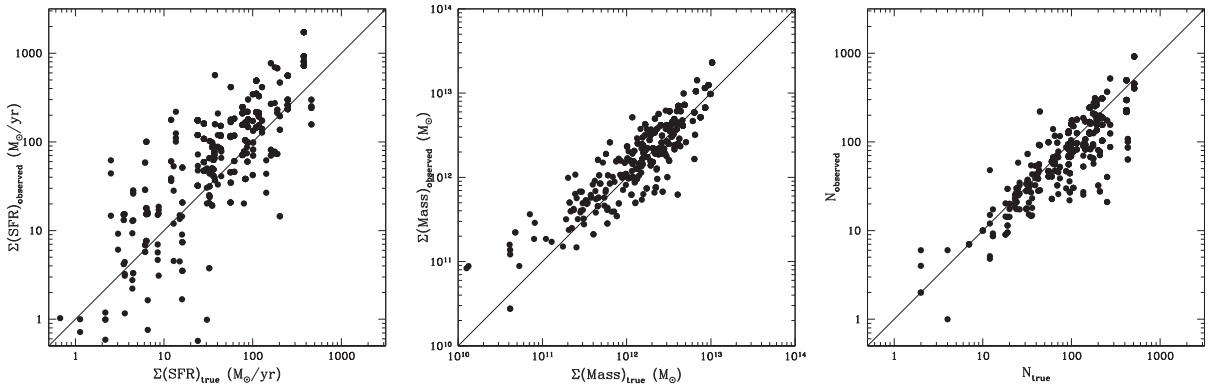

Figure 9. From left to right, 'true' values of total SFR, total stellar masses and halo occupation number of the groups versus our estimates in the 'incomplete catalogues' with the same level of spectroscopic incompleteness of the surveys used in this work.

Table 1. This table presents all the best-fitting results of the ordinary least-squares regression method performed on the low and high galaxy group sample. The first column indicates the considered *x*–*y* relation. The second column indicates the redshift bin. The third and fourth columns indicate the intercept and the slope, respectively, of the best fit so that $y = \text{slope}^{*}x + \text{intercept}$. The fifth column indicates the Spearman correlation coefficient and the sixth column indicates the value of the probability of the null hypothesis of no correlation among the considered quantities.

Relation	z	Intercept	Slope	Spearman ρ	Spearman P
log(M_{200})–log(ΣSFR)	0.15–0.5	$-7.68^{\pm 2.32}$	$0.68^{\pm 0.17}$	0.3	0.02
log(M_{200})–log(ΣSFR)	0.5–1.1	$-11.32^{\pm 1.52}$	$1.00^{\pm 0.11}$	0.44	4e−6
log(L_X)–log(ΣSFR)	0.15–0.5	$-14.35^{\pm 5.9}$	$0.37^{\pm 0.14}$	0.29	0.02
log(L_X)–log(ΣSFR)	0.5–1.1	$-23.22^{\pm 3.9}$	$0.59^{\pm 0.09}$	0.47	3e−7
log(σ)–log(ΣSFR)	0.15–0.5	$-1.32^{\pm 1.69}$	$1.12^{\pm 0.5}$	0.26	0.02
log(σ)–log(ΣSFR)	0.5–1.1	$-2.60^{\pm 1.00}$	$1.93^{\pm 0.4}$	0.4	6e−5
log(M_{200})–log(ΣM_*)	0.15–0.5	$-1.82^{\pm 3.23}$	$1.02^{\pm 0.24}$	0.5	2e−4
log(M_{200})–log(ΣM_*)	0.5–1.1	$-1.52^{\pm 3.67}$	$0.99^{\pm 0.25}$	0.4	1e−5
log(L_X)–log(ΣM_*)	0.15–0.5	$-14.36^{\pm 4.53}$	$0.62^{\pm 0.09}$	0.52	8e−5
log(L_X)–log(ΣM_*)	0.5–1.1	$-11.63^{\pm 4.5}$	$0.55^{\pm 0.11}$	0.38	7e−5
log(σ)–log(ΣM_*)	0.15–0.5	$7.09^{\pm 0.93}$	$1.95^{\pm 0.38}$	0.47	1e−4
log(σ)–log(ΣM_*)	0.5–1.1	$6.88^{\pm 1.06}$	$2.02^{\pm 0.42}$	0.37	8e−5
log(M_{200})–log(N)	0.15–0.5	$-8.04^{\pm 1.98}$	$0.67^{\pm 0.14}$	0.5	1e−4
log(M_{200})–log(N)	0.5–1.1	$-10.87^{\pm 1.52}$	$0.90^{\pm 0.11}$	0.57	1e−8
log(L_X)-log(N)	0.15–0.5	$-17.13^{\pm 3.65}$	$0.43^{\pm 0.08}$	0.5	5e−4
log(L_X)–log(N)	0.5–1.1	$-21.39^{\pm 2.9}$	$0.52^{\pm 0.06}$	0.51	0
log(σ)–log(N)	0.15–0.5	$-2.27^{\pm 0.73}$	$1.34^{\pm 0.31}$	0.44	1e−4
log(σ)–log(N)	0.5–1.1	$-3.39^{\pm 0.75}$	$1.81^{\pm 0.3}$	0.43	1e−6
log(M_{200})–SF fraction	0.15–0.5	$1.97^{\pm 4.08}$	$-0.11^{\pm 0.3}$	−0.25	0.35
log(M_{200})–SF fraction	0.5–1.1	$6.94^{\pm 1.9}$	$-0.45^{\pm 0.13}$	−0.49	0.002
log(L_X)–SF fraction	0.15–0.5	$2.40^{\pm 8.02}$	$-0.045^{\pm 0.18}$	−0.251	0.34
log(L_X)-SF fraction	0.5–1.1	$13.3^{\pm 3.54}$	$-0.29^{\pm 0.08}$	−0.5	0.001
log(σ)–SF fraction	0.15–0.5	$1.31^{\pm 1.0}$	$-0.33^{\pm 0.41}$	−0.25	0.34
log(σ)–SF fraction	0.5–1.1	$2.94^{\pm 0.66}$	$-0.87^{\pm 0.26}$	−0.41	0.0097

the age of the stellar population of the group galaxies in such a wide redshift bin (∼ 3 Gyr) could prevent us from observing a correlation. To check this possibility, we use as a reference sample of nearby groups the optically selected group sample of Yang et al. (2007) drawn from the SDSS. We select in particular a subsample of groups at $z < 0.085$. This is done because the SDSS spectroscopic sample is complete at masses7nbsp;$>10^{10}$ $M_\odot$ below this redshift limit (see Peng et al. 2010). As shown in the left-hand panel of Fig. 11, the total SFR and total mass of the nearby groups are strongly correlated. We do not see, however, a simple linear correlation in the log–log space but a double slope, flatter ($\Sigma\text{SFR} \propto M_{200}^{0.56\pm0.01}$) at $M_{200} < 10^{13}$ $M_\odot$ and steeper ($\Sigma\text{SFR} \propto M_{200}^{0.89\pm0.03}$) at $M_{200} > 10^{13}$ $M_\odot$. As explained by Yang, Mo & van den Bosch (2008), the break at the low-mass end can be explained by the halo occupation statistics. Indeed, we observe the same sharp break in the HOD of the Yang et al. (2007) subsample at $N(M > 10^{10}\,M_\odot) \sim 1$ (central panel of Fig. 11). This break indicates that, on average, below $M_{200} \sim 10^{13}$ $M_\odot$ only the central galaxy has a mass above $M > 10^{10}$ $M_\odot$ and satellites have lower masses. The existence of a significant correlation between ΣSFR and M_{200} in the nearby groups and in the more populated high-redshift group sample would suggest that we should likely observe a correlation also in the low-redshift bin. Thus, to check if the low number statistics and the scatter are hiding such a correlation, we perform the following test. We extract randomly 5000 times the same number of objects as in the intermediate-redshift sample from the Yang et al. (2007) subsample in the same mass range. We

Downloaded from https://academic.oup.com/mnras/article/445/3/2725/1041622 by guest on 18 December 2021

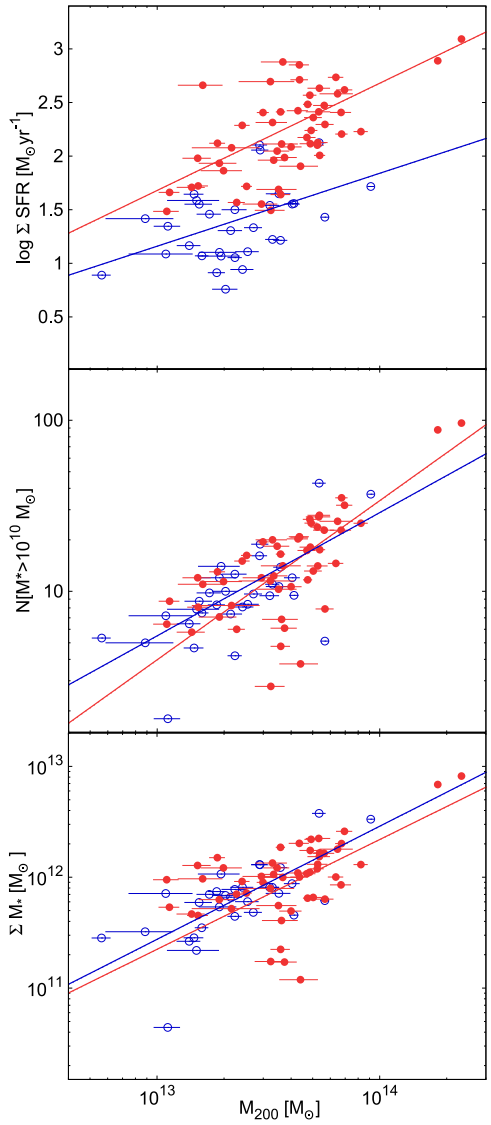

Figure 10. ΣSFR– (upper panel), HOD– (middle panel) and ΣM_*– (bottom panel) M_{200} relations for member galaxies with $M_* > 10^{10}$ M$_\odot$ in the low-z sample ($0.15 < z < 0.5$, in blue) and the high-z groups ($0.5 < z < 1.1$, in red). The blue and red lines show the best-fitting relations using the ordinary least-squares regression method presented by Akritas & Bershady (1996). The total SF activity in high-z groups is higher with respect to the low-z sample at any mass by 0.8 ± 0.12 dex. The HOD– and ΣM_*–M_{200} are consistent with a linear relation in both redshift bins with no evolution since $z \sim 1.1$.

perform for each extraction the Spearman test between ΣSFR and M_{200}. In 65 per cent of the cases, we observe a correlation between the two quantities of the same significance as in our low-redshift sample. Thus, we conclude that the mild correlation observed in our low-redshift group sample is due to low number statistics in addition to the scatter due to the width of the redshift bin.

To further check if the positive correlation between M_{200} and the redshift of the groups in the high-redshift bin can induce the positive correlation observed between ΣSFR and M_{200}, we consider the subsample of the high-z groups, described above, at $0.5 < z < 0.8$. We perform the Spearman test and the ordinary least-squares regression method (Akritas & Bershady 1996) in the log–log space of ΣSFR and M_{200} for such subsample and we find a correlation significance and slope to be perfectly consistent (within 1σ) with the results obtained with the whole high-redshift sample. The effect of the addition of the remaining $z > 0.8$ groups is only to increase the scatter of the relation by 17 per cent. Thus, we conclude that the positive correlation is not induced by a redshift bias in our group sample and that the positive correlation of the ΣSFR–M_{200} relation is real.

By comparing the ΣSFR–M_{200} relation at different redshifts, we see a clear evolution in the level of SF activity. Indeed, the total SF activity in high-redshift groups is higher with respect to the low-redshift sample. By dividing the two samples into several M_{200} bins, we estimate a mean difference of 0.8 ± 0.1 dex between high- and low-redshift groups. A milder difference (0.35 ± 0.1 dex) is observed between the [0.15–0.5] redshift bin and the groups at $z < 0.085$ of Yang et al. (2007). In order to check if this evolution is happening faster in the group galaxy population than the field population, we compare the mean SFR per galaxy in groups as a function of redshift with the mean SFR per galaxy in the whole galaxy population (Fig. 12). The mean SFR per galaxy in groups is derived by dividing the sum of the corrected ΣSFR for the groups by the sum of their corrected ΣN in the considered redshift bin. For the mean SFR per galaxy in the whole galaxy population, we use the infrared luminosity density obtained by Gruppioni et al. (2013), based on PACS data, for galaxies with mass above $M_* > 10^{10}$ M$_\odot$. Using Kennicutt (1998) relation, we convert the IR luminosity density to the SFR density. In order to obtain the mean SFR per galaxy, we divide the SFR density by the number density for $M_* > 10^{10}$ M$_\odot$ derived from the integration of the sum of the quiescent and star-forming galaxies' mass function derived by Ilbert et al. (2010). According to Fig. 12, group galaxies have very similar level of SF activity with the whole galaxy population at $z \sim 1$, but at lower redshifts they experience much faster evolution than the global relation. Since the whole galaxy population should be dominated by lower mass haloes, $M_{200} \sim 10^{12\text{–}12.5}$ M$_\odot$ according to the predicted dark matter halo mass function (e.g. Jenkins et al. 2001; Tinker et al. 2008) and to the estimate of Eke et al. (2005), this would imply that the level of SF activity is declining more rapidly since $z \sim 1$ in the more massive haloes than in the more common lower mass haloes consistent with Ziparo et al. (2014). This confirms a 'halo downsizing' effect as discussed in Popesso et al. (2012). In addition, as discussed above, we also point out that the result does not change if we do not calibrate SFR$_{\rm SED}$ (see Section 2.3.1). The effect of this calibration is just to slightly reduce the scatter of the relation.

The central and bottom panels of Fig. 10 show the HOD and the ΣM_*–M_{200} relations in the two redshift bins. In these cases, we see a very tight relation in both samples as confirmed by a Spearman test at the 99 per cent confidence level (see Table 1). This is not surprising. Indeed, while the stellar mass function of the galaxy population, and of the group galaxy population in particular, is not evolving significantly since redshift $\sim$1 as shown in Ilbert et al. (2010) and Giodini et al. (2012), respectively, the SF activity of the Universe is dropping down by an order of magnitude in the same time window (see e.g. Magnelli et al. 2013 for the whole galaxy population; Popesso et al. 2012 for groups and clusters in particular). As a consequence, the spread in ΣSFR is much higher than the spread of ΣM_*. Thus, we see a strong correlation between ΣM_* and M_{200} and only a mild correlation between ΣSFR and M_{200}.

The HOD is consistent with a linear relation in the high-redshift bin and marginally consistent with it (within 2.5σ, see Table 1) in the low-redshift bin. This is probably due to a bias induced by

Downloaded from https://academic.oup.com/mnras/article/445/3/2725/1041622 by guest on 18 December 2021

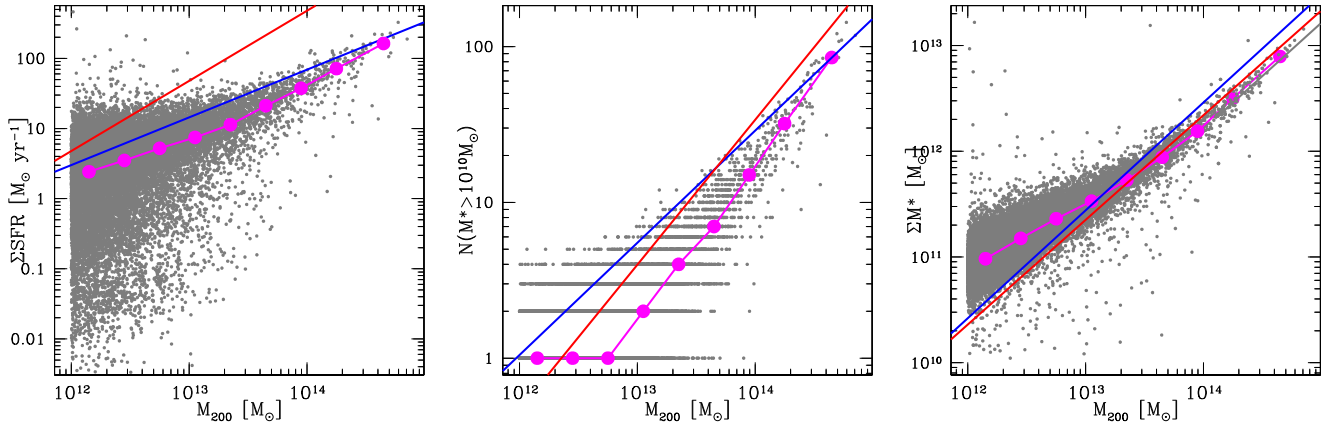

Figure 11. ΣSFR– (left-hand panel), HOD– (middle panel) and ΣM_*- (right-hand panel) M_{200} relations for a subsample of Yang et al. (2007) optically selected catalogue at $z < 0.085$ (grey points). The magenta points connected by the solid line show the median per bin of M_{200} in the Yang et al. (2007) subsample. The blue solid lines show the best-fitting relation of our low-z sample and the red solid lines show the best-fitting relation of our high-z group sample. The ΣSFR and total mass of the nearby groups are strongly correlated. We do not see, however, a simple linear correlation in the log–log space but a double slope, flatter ($\Sigma\mathrm{SFR} \propto M_{200}^{0.56\pm0.01}$) at $M_{200} < 10^{13}\,\mathrm{M}_\odot$ and steeper ($\Sigma\mathrm{SFR} \propto M_{200}^{0.89\pm0.03}$) at $M_{200} > 10^{13}\,\mathrm{M}_\odot$.

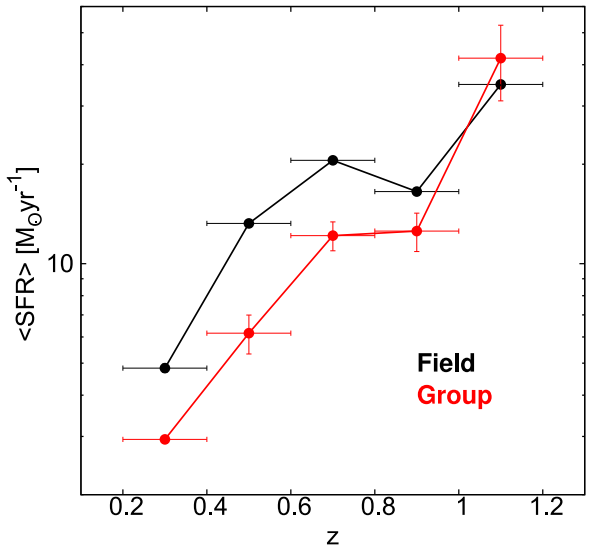

Figure 12. Mean SFR as a function of redshift. Black points show the mean of SFR for galaxies in the whole galaxy population and the red points and the error bars indicate the mean SFR in bins of redshift and respective errors in the mean.

our selection of groups with more than five members, needed to properly define the group redshift and membership. Indeed, this cut makes more likely that we favour the selection of rich groups for a given mass, in particular among the low-mass groups. Since the mean M_{200} of the low-redshift sample is a factor of 2 lower than the mean mass of the high-redshift sample, this bias is more significant in the low-redshift sample at low masses, leading to a sub-linear HOD. Indeed, the HOD obtained using the Yang et al. (2007) group subsample at $z < 0.085$ and with the same stellar mass cut is highly consistent with a linear relation for haloes with masses $M_{200} > 10^{13}\,\mathrm{M}_\odot$ as discussed above (see the central panel of Fig. 11). As for the ΣSFR–M_{200} relation, also the ΣM_*–M_{200} relation shows a double slope, $\Sigma M_* \propto M_{200}^{0.61\pm0.002}$ at $M_{200} < 10^{13}\,\mathrm{M}_\odot$ and $\Sigma M_* \propto M_{200}^{1.00\pm0.07}$ at $M_{200} > 10^{13}\,\mathrm{M}_\odot$. Since the Yang et al. (2007) groups with masses below $M_{200} < 10^{13}\,\mathrm{M}_\odot$ typically contain only the central galaxy, the relation below this limit shows actually the mean relation between the central galaxy stellar mass and the halo mass. We should note that different fitting methods on our sample lead to perfectly consistent results.

We point out that, according to Popesso et al. (2007), groups exhibit a much flatter radial density profile with respect to more massive systems. Thus, the correction for projection effects for groups should be higher than that for more massive systems. However, our sample covers a much lower and narrower mass range with respect to the one of Popesso et al. (2007) and we do not know accurately the radial density profile of our group sample. We point out that the correction is of the order of 20–15 per cent and it would not change significantly our results given the relatively large error on the slope of the relation. We also notice that the slope of the observed relation is consistent with the one observed in galaxy clusters at much higher masses (Marinoni & Hudson 2002; Pisani, Ramella & Geller 2003; Lin, Mohr & Stanford 2004; Popesso et al. 2007).

We do not observe any evolution in the HOD since $z \sim 1.1$. Similarly, we do not observe evolution in the relation between the total stellar mass in groups and the total mass, in agreement with the results of Giodini et al. (2012) (see the bottom panel of Fig. 10 and the right-hand panel of Fig. 11).

The picture emerging from Figs 10 and 11 is that accretion of galaxies or stellar mass goes together with accretion of total halo mass. Since the massive haloes are not predicted to increase their total halo mass by a large factor (Stewart et al. 2008; Fakhouri, Ma & Boylan-Kolchin 2010; Moster, Naab & White 2013) through a merger event in the last 10 Gyr, thus, the same is true for their stellar mass and number of galaxies. This picture in addition to Fig. 12 implies that the most evident evolution of the galaxy population of the most massive systems is in terms of the quenching of their SF activity. This also implies that the group galaxy population should progressively move from high to low specific SFR from $z \sim 1$ to $z \sim 0$ and move away from the MS more rapidly than galaxies in lower mass haloes, in agreement with the result of Ziparo et al. (2014).

4.2 Fraction of MS galaxies versus M_{200} and velocity dispersion

Often the level of SF activity in groups and clusters is estimated through the fraction of star-forming galaxies. In order to compare with previous results, we analyse in this section the evolution of

Downloaded from https://academic.oup.com/mnras/article/445/3/2725/1041622 by guest on 18 December 2021

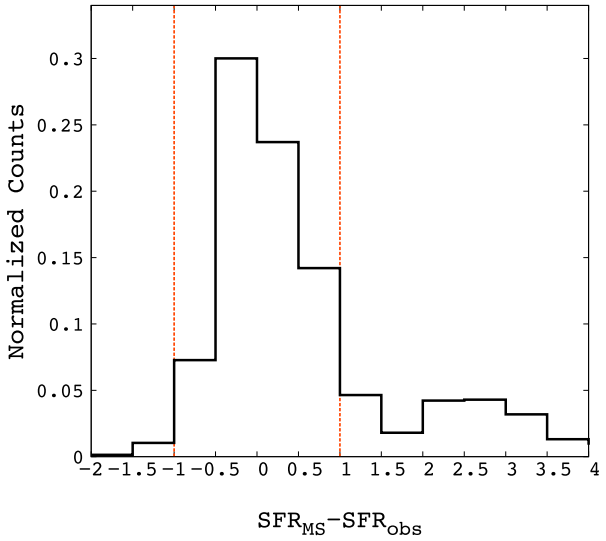

Figure 13. Normalized distribution of differences between MS SFR and observed SFR of member galaxies (ΔSFR). The red vertical lines show our limit for separation of MS member galaxies.

the fraction of star-forming galaxies as a function of the group halo mass. We define the star-forming galaxies as the ones lying on the MS (Elbaz et al. 2007). In order to identify the MS at different redshifts, we extrapolate the MS relation at the mean redshift of each redshift bin by interpolating the MS relation of Peng et al. (2010), Noeske et al. (2007) and Elbaz et al. (2007). According to these works, the scatter of the relation is ~ 0.3 dex. Fig. 13 illustrates the distribution of the residual $\Delta(\mathrm{SFR}) = \mathrm{SFR_{MS}} - \mathrm{SFR_{observed}}$, where $\mathrm{SFR_{MS}}$ is the SFR given by the MS relation at a given mass and $\mathrm{SFR_{observed}}$ is the observed SFR of a galaxy at that mass. The distribution shows a well-known bimodal distribution with the Gaussian representing the MS location with peak around 0 residual and a tail of quiescent/low star-forming galaxies at high positive values of ΔSFR. This distribution is reminiscent of the bimodal behaviour of the $U - R$ galaxy colour distribution observed by Strateva et al. (2001) in the SDSS galaxy sample. At all redshifts, the value $\Delta\mathrm{SFR} = 1$ turns out to be the best separation for MS galaxies. It is also consistent with 3σ of MS uncertainty.

The fraction of star-forming galaxies is, then, defined as the ratio between the number of SF galaxies with $M_* > 10^{10}\,\mathrm{M}_\odot$ and the total number of galaxies with $M_* > 10^{10}\,\mathrm{M}_\odot$. We apply the same spectroscopic incompleteness correction for the number of star-forming galaxies as for the total number of galaxies, so it is cancelled from the fraction. We do not find any correlation in the low-redshift bin with the halo mass (see Table 1 and Fig. 14). This is confirmed also by a lack of correlation in the Yang et al. (2007) group subsample at $z < 0.085$. We observe a significant anticorrelation with the halo mass in the high-redshift bin, as confirmed by a Spearman test (see Fig. 15). Fig. 16 shows the relation between fraction of star-forming galaxies and velocity dispersion for the galaxy groups with more than 10 spectroscopic members for which we have a reasonable estimate of the galaxy velocity dispersion. The magenta line in Fig. 16 is the upper envelope of Poggianti et al. (2006) for the ESO Distant Cluster Survey (EDisCS) clusters and groups at $z = 0.4$–0.8. Even in this case, high-mass systems seem to be already evolved at $z \sim 1$ by showing a fraction of star-forming galaxies consistent with the low-redshift counterparts at $z < 0.085$, where we measure a mean constant fraction of SF galaxies of 0.28 ± 0.5.

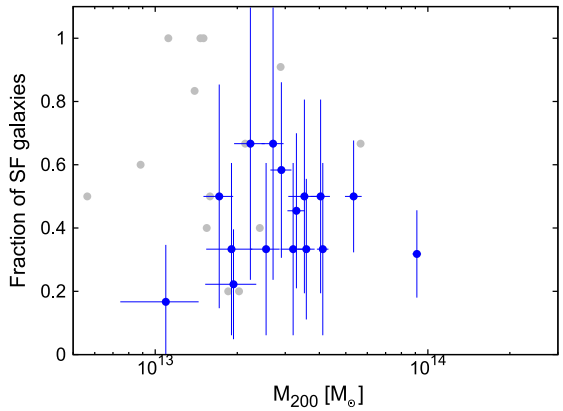

Figure 14. Fraction of star-forming galaxies as a function of halo mass for the low-z sample with more than 10 members (blue points) and less than 10 members (in grey). The Spearman test confirms no correlation for this sample.

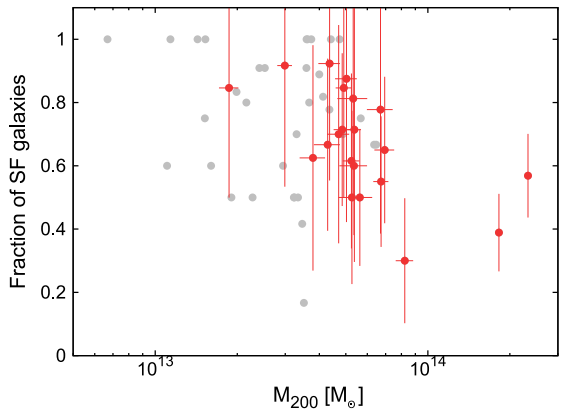

Figure 15. Fraction of star-forming galaxies as a function of halo mass for the high-z sample with more than 10 members (red points) and less than 10 members (in grey). The Spearman test confirms a significant anticorrelation for the this sample.

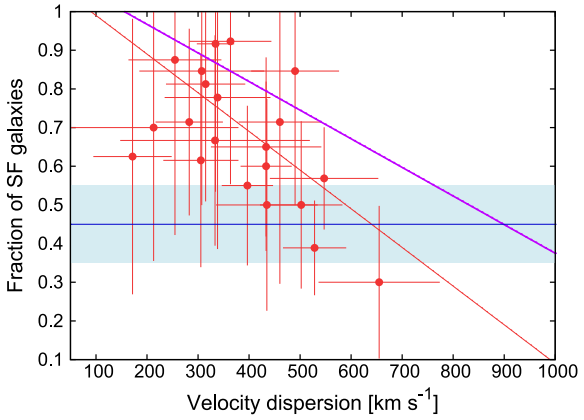

Figure 16. Fraction of star-forming galaxies versus velocity dispersion for groups in the high-z sample with more than 10 spectroscopic members. The magenta line is the upper envelope of Poggianti et al. (2006) for the EDisCS clusters and groups at $z = 0.4$–0.8. The horizontal blue line and the shaded blue area show the median fraction of star-forming galaxies and its corresponding 1σ error in low-z groups.

Downloaded from https://academic.oup.com/mnras/article/445/3/2725/1041622 by guest on 18 December 2021

Given the almost linear relation between the ΣSFR and M_{200} in the high-z sample, this implies that most of the contribution to the total SFR of the most massive systems ($M_{200} \sim 10^{14}$ M$_\odot$) is given by few but highly star-forming galaxies, while in lower mass systems ($M_{200} \sim 10^{13}$ M$_\odot$) it is given by more star-forming galaxies of average activity. Thus, this would still indicate a faster evolution in the more massive systems in terms of SF activity with respect to lower mass groups.

4.3 Comparison with the mock catalogue

To compare our results with theory, we look at the results based on the mock catalogue of the Millennium Simulation as described in Section 2.6. We analyse the same relations studied in our work by extracting from the mock catalogue a sample of groups in the same mass range and redshift range adopted in our study. The quantities ΣM_*, ΣSFR and number of galaxies per halo mass are calculated by following the same criteria as used for the real data set. In addition, we also estimate the properties of the groups at $1 < z < 2$ to completely follow the evolutionary trends of galaxies up to $z \sim 2$. Fig. 17 shows the predictions of the same relations presented in Fig. 10. The top panel of the figure shows the total SFR of the mock groups as a function of their halo masses. As already known, the semi-analytical models of the Millennium Simulation underpredict the level of SF activity of the galaxy population and, in particular, of the group and cluster galaxies. Indeed, even the level of activity of the high-redshift groups is well below the level of the low-redshift groups of our sample (dotted blue line in the plot). This class of models assumes that, when galaxies are accreted on to a more massive system, the associated hot gas reservoir is stripped instantaneously. This, in addition to the AGN feedback, induces a very rapid decline of the SF histories of satellite galaxies, and contributes to create an excess of red and passive galaxies with respect to the observations (e.g. Wang et al. 2007). More recent high-resolution simulations do not help in improving the results (Guo et al. 2011; Weinmann, Neistein & Dekel 2011). This is known as the 'overquenching problem' for satellites galaxies. Over 95 per cent of the cluster and group galaxies within the virial radius in the local simulated universe are passive (Guo et al. 2011), at odds with observations (e.g. Popesso et al. 2005; Weinmann et al. 2006; Hansen et al. 2009; Kimm et al. 2009; Liu et al. 2010). Indeed, as Fig. 18 shows, galaxies in mock groups reside under the MS in any redshift bin, indicating that the evolution even in group galaxies is happening at $z > 2$. This is at odds with our results since in the previous section we have shown that in the low-mass groups most of the galaxies above 10^{10} M$_\odot$ are MS galaxies.

We do not observe any evolution in the HOD (central panel of Fig. 17), which is also consistent quantitatively with the HOD observed in our group sample. In the same way, we do not observe any evolution in the ΣM_*–M_{200} relation but we also observe a quantitative discrepancy with respect to observations. Indeed, at any redshift the total stellar mass in groups is underpredicted with respect to the observed one. This is understandable given the much lower SFR of the simulated group galaxies with respect to the observations, which limits the galaxy stellar mass growth.

5 SUMMARY AND CONCLUSION

In this paper, we provide an analysis of the evolution of the total SF activity, total stellar mass and HOD by using one of the largest X-ray selected samples of galaxy groups with secure spectroscopic

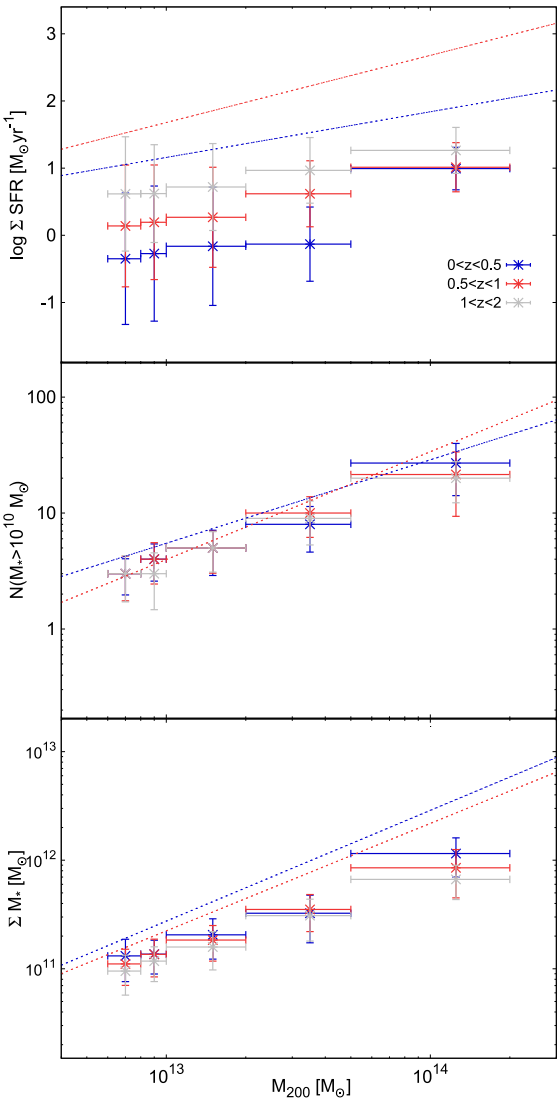

Figure 17. ΣSFR– (upper panel), HOD– (middle panel) and ΣM_*– (bottom panel) M_{200} relations for the groups with $0 < z < 0.5$ (in red) and $0.5 < z < 1$ (in blue) and with $1 < z < 2$ (in grey) for the mock catalogue. The dashed lines show the results based on the observations.

identification on the major deep field surveys (ECDF, CDFN, COSMOS, AEGIS) up to $z \sim 1.1$. We first check the robustness of our method in determining the group velocity dispersion and membership extensively using mock catalogues and check the possible biases induced by the spectroscopic incompleteness of the surveys used in our analysis. We show that for a robust measurement of the group velocity dispersion and group membership definition, a first guess of the velocity dispersion derived from the X-ray luminosity is essential for a reliable result. We compare our results with the one based on an optically selected sample of groups at $z < 0.085$ in order to fully follow the evolution of the galaxy population in groups to the local Universe. We list below our main results.

(1) We observe a clear evolution in the level of SF activity in galaxy groups. Indeed, the total SF activity in high-redshift groups ($0.5 < z < 1.1$) is higher with respect to the low-redshift sample ($0.15 < z < 0.5$) at any mass by almost 0.8 ± 0.1 dex. A milder difference (0.35 ± 0.1 dex) is observed between the [0.15–0.5] redshift bin and the groups at $z < 0.085$. This

Downloaded from https://academic.oup.com/mnras/article/445/3/2725/1041622 by guest on 18 December 2021

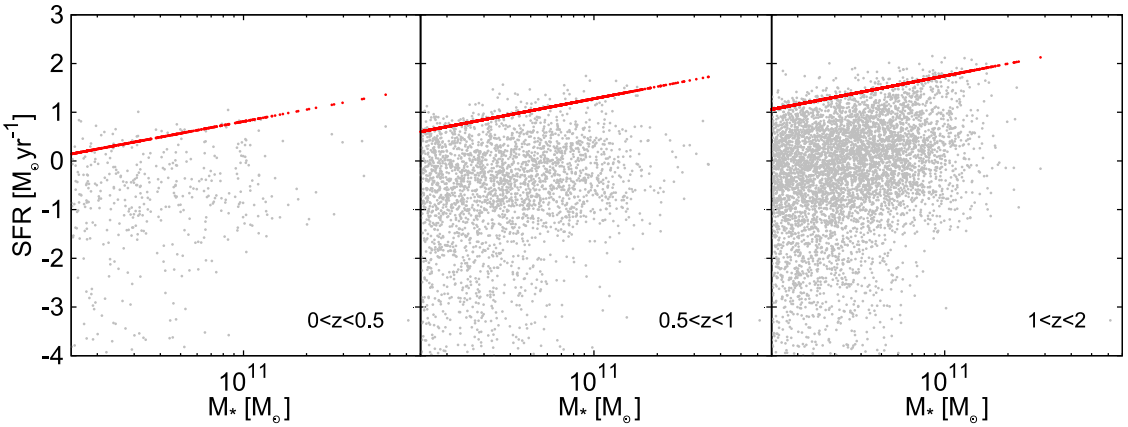

Figure 18. SFR as a function of stellar mass for the member galaxies in the mock catalogue. The red points show the position of the MS for the lowest redshift ($z = 0$, 0.5 and 1 from left to right, respectively) in each bin.

evolution seems to be much faster than the one observed in the whole galaxy population (Gruppioni et al. 2013), dominated by lower mass haloes ($M_{200} \sim 10^{12–12.5}$ M$_\odot$; Jenkins et al. 2001; Eke et al. 2005; Tinker et al. 2008). This would imply that the level of SF activity is declining more rapidly since $z \sim 1.1$ in the more massive haloes than in the more common lower mass haloes, confirming a 'halo downsizing' effect as discussed by Popesso et al. (2012).

(2) The HOD and the total stellar mass–M_{200} relation are consistent with a linear relation in all redshift bins in the M_{200} range considered in our analysis. We do not observe any evolution in the HOD since $z \sim 1$. Similarly, we do not observe evolution in the relation between the total stellar mass in groups and the total mass, in agreement with the results of Giodini et al. (2012). The picture emerging from our findings is that massive groups at $M_{200} \sim 10^{13–14}$ M$_\odot$ have already accreted the same amount of mass and have the same number of galaxies as the low-redshift counterparts, as predicted by Stewart et al. (2008). This implies that the most evident evolution of the galaxy population of the most massive systems acts in terms of quenching their galaxy SF activity. This also implies that the group galaxy population should progressively move from high to low specific SFRs from $z \sim 1$ to $z \sim 0$ and rapidly move away from the MS since $z \sim 1$ consistent with the recent results of Ziparo et al. (2013) based on a similar data set.

(3) The analysis of the evolution of the fraction of SF galaxies as a function of halo mass or velocity dispersion shows that high-mass systems seem to be already evolved at $z \sim 1$ by showing a fraction of star-forming galaxies consistent with the low-redshift counterparts at $z < 0.085$. Given the almost linear relation between the ΣSFR and M_{200} in the high-z sample, this implies that most of the contribution to the total SFR of the most massive systems ($M_{200} \sim 10^{14}$ M$_\odot$) is given by few highly star-forming galaxies, while in lower mass systems ($M_{200} \sim 10^{13}$ M$_\odot$) it is given by many galaxies of average activity. This would be an additional sign of a faster evolution in the more massive systems in terms of SF activity with respect to lower mass groups. Thus, it would confirm the 'halo downsizing' effect.

(4) The comparison of our results with the prediction of the Millennium Simulation semi-analytical model confirms the known problem of the models. We confirm the strong bias due to the 'satellite overquenching' problem in suppressing significantly the SF activity of group galaxies (more than an order of magnitude) at any redshift with respect to observations. The HOD predicted by the simulations is remarkably in agreement with the observations. But due to the low SF activity of galaxies in massive haloes, the models also predict a lower total stellar mass in groups with respect to the observed one at any redshift.

Our results support a scenario in which the quenching of SF occurs earlier in galaxies embedded in more massive haloes, though we are considering a quite narrow halo mass range. This would be consistent with the results obtained by Popesso et al. (2012) in a similar redshift range but in a broader mass range, which includes also galaxy clusters. Other pieces of evidence in the literature support the differential evolution of the SF activity in massive haloes with respect to the field or lower mass haloes. For instance, the formation of the galaxy red sequence, which leads to the local dichotomy between red and blue galaxies, happens earlier in groups than in the field especially at high stellar masses (Wilman et al. 2009; Iovino et al. 2010; Kovač et al. 2010; Wilman & Erwin 2012; Mok et al. 2013). Morphological transformations are in place in groups at $z < 1$, leading to a transient population of 'red spirals' not observed in the field (Balogh et al. 2009; Wolf et al. 2009; Mei et al. 2012). There is also evidence that at $z \sim 1$ there is a flattening of the SFR–density relation (Elbaz et al. 2007; Cooper et al. 2008; Popesso et al. 2011; Ziparo et al. 2014) with respect to the local anticorrelation. Ziparo et al. (2014) find on the very same data set that the differential evolution of the groups galaxies with respect to field is due to the fact that star-forming group galaxies are perfectly on the MS at $z \sim 1$ whereas at lower redshift they are quenched, thus, dropping off the MS quicker than field galaxies towards the region of SF quiescence.

What is causing this differential evolution as a function of the halo mass? According to Peng et al. (2010) massive galaxies, as the ones considered in our sample, evolve mostly because of an internally driven process, called 'mass quenching', caused perhaps by feedback from active galactic nuclei. But since this process is unlikely to be more efficient in quenching SF of massive galaxies in massive haloes than in other environments as the stellar mass functions do not change significantly in groups with respect to field (Giodini et al. 2012), the 'environmental quenching' must be the main mechanism for quenching the SF of the most massive satellites in massive haloes. Which kind of process is causing this 'environmental quenching' is still quite unknown. Ram-pressure stripping (Gunn & Gott 1972) and starvation (Larson, Tinsley & Caldwell 1980) are two plausible candidates for producing this quenching. Ram-pressure stripping 'quenches' SF immediately (Abadi, Moore & Bower 1999) as it can sweep interstellar medium out of a galaxy. Starvation, caused by the removal of the hot gas halo reservoirs

Downloaded from https://academic.oup.com/mnras/article/445/3/2725/1041622 by guest on 18 December 2021

of galaxies which leads to a cut in the supply of cold gas in the galaxy, is also a likely candidate. Tidal galaxy–galaxy encounters or the interaction with the intracluster/intragroup medium can lead to the removal of galaxy hot gas reservoirs which induce starvation. Therefore, starvation should quench SF earlier in more massive haloes than in low-mass haloes, as we observe.

Cen (2011) proposes that this differential evolution could be explained simply in terms of the current theory of gas accretion that hinges on the cold and hot two-mode accretion model (Kereš et al. 2005; Dekel & Birnboim 2006). The halo mass is the main determinant of gas accretion: large haloes primarily accrete hot gas while small haloes primarily accrete cold gas. The overall heating of cosmic gas due to formation of large haloes (such as groups and clusters) and large-scale structure causes a progressively larger fraction of haloes to inhabit regions where gas has too high entropy to cool to continue feeding the residing galaxies. The combined effect is differential in that overdense regions are heated earlier and to higher temperatures than lower density regions at any given time. Because larger haloes tend to reside in more overdense regions than smaller haloes, the net differential effects would naturally lead to both the standard galaxy downsizing effect and the halo downsizing effect.

The current analysis cannot provide evidence in favour of one of these scenarios. Further analysis must be conducted to study the cold gas content of galaxies in haloes of different masses, to distinguish between the different possibilities and identify the process responsible for the 'environmental quenching'.

ACKNOWLEDGEMENTS

GE acknowledges the support from and participation in the International Max-Planck Research School on Astrophysics at the Ludwig-Maximilians University. MLB acknowledges financial support from an NSERC Discovery Grant, and from NWO and NOVA grants that supported his sabbatical at the University of Leiden, where this work was completed. PACS has been developed by a consortium of institutes led by MPE (Germany) and including UVIE (Austria); KUL, CSL, IMEC (Belgium); CEA, OAMP (France); MPIA (Germany); IFSI, OAP/AOT, OAA/CAISMI, LENS, SISSA (Italy); IAC (Spain). This development has been supported by the funding agencies BMVIT (Austria), ESA-PRODEX (Belgium), CEA/CNES (France), DLR (Germany), ASI (Italy), and CICYT/MCYT (Spain).

This research has made use of NASA's Astrophysics Data System, of NED, which is operated by JPL/Caltech, under contract with NASA, and of SDSS, which has been funded by the Sloan Foundation, NSF, the US Department of Energy, NASA, the Japanese Monbukagakusho, the Max Planck Society and the Higher Education Funding Council of England. The SDSS is managed by the participating institutions (www.sdss.org/collaboration/credits.html).

We gratefully acknowledge the contributions of the entire COSMOS collaboration consisting of more than 100 scientists. More information about the COSMOS survey is available at http://www.astro.caltech.edu/cosmos. This project has been supported by the DLR grant 50OR1013 to MPE.

REFERENCES

Abadi M. G., Moore B., Bower R. G., 1999, MNRAS, 308, 947
Akritas M. G., Bershady M. A., 1996, ApJ, 470, 706
Alexander D. M. et al., 2003, AJ, 126, 539
Allevato V. et al., 2012, ApJ, 758, 47
Balogh M. L. et al., 2009, MNRAS, 398, 754
Balogh M. L. et al., 2011, MNRAS, 412, 2303
Barger A. J., Cowie L. L., Wang W.-H., 2008, ApJ, 689, 687
Barmby P., Huang J.-S., Ashby M. L. N., Eisenhardt P. R. M., Fazio G. G., Willner S. P., Wright E. L., 2008, ApJS, 177, 431
Bauer F. E. et al., 2002, AJ, 123, 1163
Beers T. C., Flynn K., Gebhardt K., 1990, AJ, 100, 32
Berta S. et al., 2010, A&A, 518, L30
Berta S. et al., 2013, A&A, 551, A100
Bielby R. M. et al., 2010, A&A, 523, A66
Bielby R. et al., 2012, A&A, 545, A23
Blanton M. R. et al., 2005, AJ, 129, 2562
Brimioulle F., Lerchster M., Seitz S., Bender R., Snigula J., 2008, preprint (arXiv:0811.3211)
Brinchmann J., Charlot S., White S. D. M., Tremonti C., Kauffmann G., Heckman T., Brinkmann J., 2004, MNRAS, 351, 1151
Buat V., Takeuchi T. T., Burgarella D., Giovannoli E., Murata K. L., 2009, A&A, 507, 693
Bundy K. et al., 2006, ApJ, 651, 120
Capak P. L., 2009, BAAS, 41, 708
Capak P. et al., 2007, ApJS, 172, 99
Cardamone C. N. et al., 2010, ApJS, 189, 270
Carlberg R. G., Yee H. K. C., Ellingson E., 1997, ApJ, 478, 462
Cen R., 2011, ApJ, 741, 99
Chabrier G., 2003, PASP, 115, 763
Cimatti A. et al., 2008, A&A, 482, 21
Coil A. L., Newman J. A., Kaiser N., Davis M., Ma C.-P., Kocevski D. D., Koo D. C., 2004, ApJ, 617, 765
Coil A. L. et al., 2009, ApJ, 701, 1484
Cooper M. C. et al., 2007, MNRAS, 376, 1445
Cooper M. C. et al., 2008, MNRAS, 383, 1058
Cooper M. C., Gallazzi A., Newman J. A., Yan R., 2010, MNRAS, 402, 1942
Cooper M. C. et al., 2011, ApJS, 193, 14
Cooper M. C. et al., 2012, MNRAS, 419, 3018
Croton D. J. et al., 2006, MNRAS, 365, 11
Damen M. et al., 2011, ApJ, 727, 1
Davis M., Geller M. J., 1976, ApJ, 208, 13
Davis M. et al., 2003, in Guhathakurta P., ed., in Proc. SPIE Conf. Ser. Vol. 4834, Discoveries and Research Prospects from 6- to 10-Meter-Class Telescopes II. SPIE, Bellingham, p. 161
Davis M. et al., 2007, ApJ, 660, L1
De Lucia G., Springel V., White S. D. M., Croton D., Kauffmann G., 2006, MNRAS, 366, 499
De Lucia G., Weinmann S., Poggianti B. M., Aragón-Salamanca A., Zaritsky D., 2012, MNRAS, 423, 1277
Dekel A., Birnboim Y., 2006, MNRAS, 368, 2
Di Matteo T., Springel V., Hernquist L., 2005, Nature, 433, 604
Dressler A., 1980, ApJ, 236, 351
Efron B., 1982, The Jackknife, the Bootstrap and Other Resampling Plans. SIAM, Philadelphia
Eke V. R., Baugh C. M., Cole S., Frenk C. S., King H. M., Peacock J. A., 2005, MNRAS, 362, 1233
Elbaz D. et al., 2007, A&A, 468, 33
Elbaz D. et al., 2011, A&A, 533, A119
Elvis M. et al., 2009, ApJS, 184, 158
Erfanianfar G. et al., 2013, ApJ, 765, 117
Fakhouri O., Ma C.-P., Boylan-Kolchin M., 2010, MNRAS, 406, 2267
Finn R. A. et al., 2010, ApJ, 720, 87
Finoguenov A. et al., 2007, ApJS, 172, 182
Finoguenov A. et al., 2009, ApJ, 704, 564
Finoguenov A. et al., 2010, MNRAS, 403, 2063
Gao L., White S. D. M., Jenkins A., Stoehr F., Springel V., 2004, MNRAS, 355, 819
Geller M. J., Huchra J. P., 1983, ApJS, 52, 61
George M. R. et al., 2011, ApJ, 742, 125

Downloaded from https://academic.oup.com/mnras/article/445/3/2725/1041622 by guest on 18 December 2021

George M. R., Ma C.-P., Bundy K., Leauthaud A., Tinker J., Wechsler R. H., Finoguenov A., Vulcani B., 2013, ApJ, 770, 113
Giavalisco M. et al., 2004, ApJ, 600, L93
Giodini S. et al., 2012, A&A, 538, A104
Gómez P. L. et al., 2003, ApJ, 584, 210
Grazian A. et al., 2006, A&A, 449, 951
Gruppioni C. et al., 2013, MNRAS, 432, 23
Gunn J. E., Gott I. J. R., 1972, ApJ, 176, 1
Guo Q., White S., Li C., Boylan-Kolchin M., 2010, MNRAS, 404, 1111
Guo Q. et al., 2011, MNRAS, 413, 101
Hansen S. M., Sheldon E. S., Wechsler R. H., Koester B. P., 2009, ApJ, 699, 1333
Hasinger G. et al., 2007, ApJS, 172, 29
Hogg D. W. et al., 2004, ApJ, 601, L29
Hopkins P. F., Hernquist L., Cox T. J., Di Matteo T., Robertson B., Springel V., 2006, ApJS, 163, 1
Ilbert O. et al., 2009, ApJ, 690, 1236
Ilbert O. et al., 2010, ApJ, 709, 644
Iovino A. et al., 2010, A&A, 509, A40
Jeltema T. E., Mulchaey J. S., Lubin L. M., Fassnacht C. D., 2007, ApJ, 658, 865
Jenkins A., Frenk C. S., White S. D. M., Colberg J. M., Cole S., Evrard A. E., Couchman H. M. P., Yoshida N., 2001, MNRAS, 321, 372
Kennicutt J. R. C., 1998, ARA&A, 36, 189
Kereš D., Katz N., Weinberg D. H., Davé R., 2005, MNRAS, 363, 2
Kimm T. et al., 2009, MNRAS, 394, 1131
Kitzbichler M. G., White S. D. M., 2007, MNRAS, 376, 2
Kovač K. et al., 2010, ApJ, 718, 86
Kriek M., van Dokkum P. G., Labbé I., Franx M., Illingworth G. D., Marchesini D., Quadri R. F., 2009, ApJ, 700, 221
Laird E. S. et al., 2009, ApJS, 180, 102
Larson R. B., Tinsley B. M., Caldwell C. N., 1980, ApJ, 237, 692
Le Floc'h E. et al., 2009, ApJ, 703, 222
Leauthaud A. et al., 2010, ApJ, 709, 97
Lehmer B. D. et al., 2005, ApJS, 161, 21
Lewis I. et al., 2002, MNRAS, 334, 673
Lilly S. J. et al., 2007, ApJS, 172, 70
Lilly S. J. et al., 2009, ApJS, 184, 218
Lin Y.-T., Mohr J. J., Stanford S. A., 2004, ApJ, 610, 745
Liu L., Yang X., Mo H. J., van den Bosch F. C., Springel V., 2010, ApJ, 712, 734
Lotz J. M. et al., 2008, ApJ, 672, 177
Lutz D. et al., 2011, A&A, 532, A90
Magnelli B., Elbaz D., Chary R. R., Dickinson M., Le Borgne D., Frayer D. T., Willmer C. N. A., 2009, A&A, 496, 57
Magnelli B. et al., 2013, A&A, 553, A132
Marinoni C., Hudson M. J., 2002, ApJ, 569, 101
Mei S. et al., 2012, ApJ, 754, 141
Miller N. A., Fomalont E. B., Kellermann K. I., Mainieri V., Norman C., Padovani P., Rosati P., Tozzi P., 2008, ApJS, 179, 114
Mok A. et al., 2013, MNRAS, 431, 1090
Morrison G. E., Owen F. N., Dickinson M., Ivison R. J., Ibar E., 2010, ApJS, 188, 178
Moster B. P., Naab T., White S. D. M., 2013, MNRAS, 428, 3121
Newman J. A. et al., 2013, ApJS, 208, 5
Noeske K. G. et al., 2007, ApJ, 660, L43
Padovani P., Mainieri V., Tozzi P., Kellermann K. I., Fomalont E. B., Miller N., Rosati P., Shaver P., 2009, ApJ, 694, 235
Papovich C., Dickinson M., Ferguson H. C., 2001, ApJ, 559, 620
Peng Y. et al., 2010, ApJ, 721, 193
Pisani A., Ramella M., Geller M. J., 2003, AJ, 126, 1677
Poggianti B. M. et al., 2006, ApJ, 642, 188
Poglitsch A. et al., 2010, A&A, 518, L2
Popesso P., Böhringer H., Romaniello M., Voges W., 2005, A&A, 433, 415
Popesso P., Biviano A., Romaniello M., Böhringer H., 2007, A&A, 461, 411
Popesso P. et al., 2011, A&A, 532, A145
Popesso P. et al., 2012, A&A, 537, A58
Pratt G. W., Böhringer H., Croston J. H., Arnaud M., Borgani S., Finoguenov A., Temple R. F., 2007, A&A, 461, 71
Prescott M. K. M., Impey C. D., Cool R. J., Scoville N. Z., 2006, ApJ, 644, 100
Quadri R. et al., 2007, AJ, 134, 1103
Rix H.-W. et al., 2004, ApJS, 152, 163
Rykoff E. S. et al., 2008, MNRAS, 387, L28
Sanders D. B. et al., 2007, ApJS, 172, 86
Santini P. et al., 2009, A&A, 504, 751
Scodeggio M. et al., 2009, A&A, 501, 21
Scoville N. et al., 2007, ApJS, 172, 1
Shapley A. E., Steidel C. C., Adelberger K. L., Dickinson M., Giavalisco M., Pettini M., 2001, ApJ, 562, 95
Shapley A. E., Steidel C. C., Erb D. K., Reddy N. A., Adelberger K. L., Pettini M., Barmby P., Huang J., 2005, ApJ, 626, 698
Silverman J. D. et al., 2010, ApJS, 191, 124
Springel V. et al., 2005, Nature, 435, 629
Stewart K. R., Bullock J. S., Wechsler R. H., Maller A. H., Zentner A. R., 2008, ApJ, 683, 597
Strateva I. et al., 2001, AJ, 122, 1861
Sun M., 2012, New J. Phys., 14, 045004
Sun M., Sehgal N., Voit G. M., Donahue M., Jones C., Forman W., Vikhlinin A., Sarazin C., 2011, ApJ, 727, L49
Taniguchi Y. et al., 2007, ApJS, 172, 9
Tinker J., Kravtsov A. V., Klypin A., Abazajian K., Warren M., Yepes G., Gottlöber S., Holz D. E., 2008, ApJ, 688, 709
Tran K.-V. H., Moustakas J., Gonzalez A. H., Bai L., Zaritsky D., Kautsch S. J., 2008, ApJ, 683, L17
Trump J. R. et al., 2007, ApJS, 172, 383
van den Bosch F. C., Yang X., Mo H. J., 2003, MNRAS, 340, 771
Wang L., Li C., Kauffmann G., De Lucia G., 2007, MNRAS, 377, 1419
Weinmann S. M., van den Bosch F. C., Yang X., Mo H. J., 2006, MNRAS, 366, 2
Weinmann S. M., Kauffmann G., van den Bosch F. C., Pasquali A., McIntosh D. H., Mo H., Yang X., Guo Y., 2009, MNRAS, 394, 1213
Weinmann S. M., Neistein E., Dekel A., 2011, MNRAS, 417, 2737
Willner S. P. et al., 2012, ApJ, 756, 72
Wilman D. J., Erwin P., 2012, ApJ, 746, 160
Wilman D. J. et al., 2005, MNRAS, 358, 88
Wilman D. J., Oemler J. A., Mulchaey J. S., McGee S. L., Balogh M. L., Bower R. G., 2009, ApJ, 692, 298
Wilman D. J., Fontanot F., De Lucia G., Erwin P., Monaco P., 2013, MNRAS, 433, 2986
Wolf C. et al., 2009, MNRAS, 393, 1302
Wright N. J., Drake J. J., Civano F., 2010, ApJ, 725, 480
Wuyts S. et al., 2011, ApJ, 742, 96
Xue Y. Q. et al., 2011, ApJS, 195, 10
Yang X., Mo H. J., van den Bosch F. C., 2003, MNRAS, 339, 1057
Yang X., Mo H. J., Jing Y. P., van den Bosch F. C., Chu Y., 2004, MNRAS, 350, 1153
Yang X., Mo H. J., van den Bosch F. C., Jing Y. P., 2005, MNRAS, 356, 1293
Yang X., Mo H. J., van den Bosch F. C., Pasquali A., Li C., Barden M., 2007, ApJ, 671, 153
Yang X., Mo H. J., van den Bosch F. C., 2008, ApJ, 676, 248
Ziparo F. et al., 2013, MNRAS, 434, 3089
Ziparo F. et al., 2014, MNRAS, 437, 458

APPENDIX A: X-RAY GROUPS OF GALAXIES IN CDFN

The catalogue of X-ray groups follows the original results of Bauer et al. (2002), based on the first 1 Ms *Chandra* data. The main difference in the catalogue consists in a self-consistent use of the flux at R_{500} or larger apertures for the flux extraction. This allows us to use our calibrations of group masses, provided by COSMOS (Leauthaud et al. 2010) and ECDFS (Finoguenov et al., submitted)

Downloaded from https://academic.oup.com/mnras/article/445/3/2725/1041622 by guest on 18 December 2021

Table A1. X-ray group catalogue: (1) X-ray ID; (2) RA (deg); (3) Dec. (deg); (4) z; (5) flux (10^{-15} erg cm^{-2} s^{-1}); (6) L_X(0.1–2.4 keV)(10^{42} erg s^{-1}); (7) M_{200} (10^{13} M$_\odot$); (8) r_{200} (deg); (9) flag; (10) flux significance; (11) velocity dispersion from X-ray luminosities (km s^{-1}); (12) $N(z)$.

ID	RA	Dec.	z	Flux	L_X	M_{200}	r_{200}	Flux significance	Flag	Velocity dispersion	$N(z_{spec})$
(1)	(2)	(3)	(4)	(5)	(6)	(7)	(8)	(9)	(10)	(11)	(12)
2	189.456 19	62.363 14	0.398	1.26 ± 0.36	1.21 ± 0.34	2.16 ± 0.35	0.0262	3.52	3	229	0
4	189.260 89	62.351 24	0.800	0.54 ± 0.17	3.60 ± 1.12	2.94 ± 0.52	0.0177	3.19	1	277	9
5	188.863 85	62.353 66	0.652	1.91 ± 0.57	6.32 ± 1.89	4.69 ± 0.79	0.0238	3.34	3	319	0
6	189.362 76	62.323 81	0.277	0.84 ± 0.19	0.34 ± 0.08	1.12 ± 0.15	0.028	4.22	2	176	9
7	189.482 84	62.255 52	0.455	2.99 ± 0.24	3.83 ± 0.31	4.12 ± 0.19	0.0294	12.22	1	293	14
8	189.184 99	62.264 16	0.850	1.38 ± 0.17	8.92 ± 1.07	4.85 ± 0.34	0.0202	8.36	1	336	46
9	188.988 03	62.2646	0.375	1.07 ± 0.28	0.88 ± 0.23	1.82 ± 0.27	0.0259	3.78	3	214	3
10	189.073 92	62.260 07	1.999	0.39 ± 0.85	36.09 ± 7.74	4.41 ± 0.54	0.0119	4.66	2	402	3
13	189.0872	62.186 05	1.014	0.51 ± 0.18	7.12 ± 2.58	3.67 ± 0.75	0.0164	2.76	1	314	20
14	189.5959	62.1628	0.914	1.24 ± 0.32	$10.77\text{E} \pm 2.74$	5.13 ± 0.75	0.0196	3.92	3	348	0
15	189.333 36	62.128 23	0.943	0.76 ± 0.17	7.80 ± 1.71	4.13 ± 0.52	0.0179	4.56	3	323	0
16	189.137 75	62.150 06	0.840	0.48 ± 0.12	3.77 ± 0.93	2.92 ± 0.41	0.0171	4.05	1	279	12
17	189.042 09	62.147 11	1.139	0.61 ± 0.14	11.41 ± 2.52	4.37 ± 0.56	0.0162	4.52	3	343	2
19	188.961 64	62.120 97	0.491	2.49 ± 0.40	3.84 ± 0.62	4.00 ± 0.38	0.0275	6.2	3	292	0
20	189.538	62.131 81	0.948	0.64 ± 0.23	6.89 ± 2.46	3.81 ± 0.77	0.0174	2.8	3	314	0
21	188.862 26	62.102 17	0.895	1.37 ± 0.41	11.05 ± 3.41	5.30 ± 0.93	0.0201	3.24	5	351	0
22	189.113 61	62.100 88	1.217	0.45 ± 0.13	10.99 ± 3.14	4.00 ± 0.65	0.0152	3.5	3	337	1
23	189.284 45	62.090 72	0.956	0.69 ± 0.17	7.46 ± 1.88	3.97 ± 0.57	0.0175	3.96	3	319	0
24	189.020 17	62.088 88	1.217	0.91 ± 0.22	17.94 ± 4.34	5.37 ± 0.74	0.0167	4.13	5	375	0
25	189.220 03	62.070 86	0.188	4.20 ± 0.53	0.65 ± 0.08	1.75 ± 0.13	0.045	7.92	3	204	0
27	189.288 74	62.025 23	1.640	1.20 ± 0.27	46.55 ± 10.55	6.73 ± 0.88	0.0152	4.41	5	442	0
28	189.179 82	62.020 48	0.426	1.80 ± 0.42	1.98 ± 0.47	2.84 ± 0.39	0.0273	4.22	3	254	0
30	189.089 41	62.269 75	0.681	0.17 ± 0.11	0.90 ± 0.61	1.42 ± 0.52	0.0155	1.48	2	207	7
31	189.100 07	62.258 22	0.642	0.45 ± 0.28	1.71 ± 1.06	2.16 ± 0.73	0.0185	1.6	2	240	10
32	189.090 46	62.263 67	1.241	0.19 ± 0.08	6.75 ± 2.73	2.93 ± 0.66	0.0135	2.48	4	302	3
33	189.3379	62.151 65	1.126	0.49 ± 0.11	9.45 ± 2.23	3.95 ± 0.53	0.0158	4.24	3	330	0
34	189.530 13	62.119 78	0.280	1.26 ± 0.57	0.51 ± 0.23	1.41 ± 0.36	0.03	2.2	5	192	0

surveys. In columns 1, 2 and 3, we provide the group identification number, RA and Dec. of the peak of X-ray emission. In column 4, the mean of red sequence redshifts which is substituted with the median of spectroscopic redshift in case there is a spectroscopic redshift determination for the group member galaxies is given. The group flux in the 0.5–2 keV band in column 5 with the corresponding 1σ error is listed. The rest-frame luminosity in the 0.1–2.4 keV is presented in column 6. Column 7 gives the estimated total mass, M_{200}, computed following Leauthaud et al. (2010) and assuming a standard evolution of scaling relations: $M_{200}E_z = f(L_X E_z^{-1})$, where $E_z = (\Omega_M(1+z)^3 + \Omega_\Lambda)^{1/2}$, standard evolution of the scaling relation. The corresponding R_{200} in degrees is listed in column 8. Column 9 lists flux significance which provides insights into the reliability of both the source detection and the identification. Column 10 presents the flag for our identification, as described in Section 2.2. The velocity dispersion estimated from X-ray luminosities is given in column 11. The number of spectroscopic member galaxies inside $2\times R_{200}$ is given in Column 12.

[1]*Excellence Cluster Universe, Boltzmannstr. 2, D-85748 Garching bei München, Germany*
[2]*Max-Planck-Institut für extraterrestrische Physik, Giessenbachstraße 1, D-85748 Garching bei München, Germany*
[3]*Department of Physics, University of Helsinki, PO Box 64, FI-00014 Helsinki, Finland*
[4]*INAF/Osservatorio Astronomico di Trieste, via G. B. Tiepolo 11, I-34131 Trieste, Italy*
[5]*School of Physics and Astronomy, University of Birmingham, Edgbaston, Birmingham B15 2TT, UK*
[6]*Laboratoire AIM, CEA/DSM-CNRS-Université Paris Diderot, IRFU/Service d'Astrophysique, Bât.709, CEA-Saclay, F-91191 Gif-sur-Yvette Cedex, France*
[7]*National Optical Astronomy Observatory, 950 North Cherry Avenue, Tucson, AZ 85719, USA*
[8]*National Astronomical Observatory of Japan, 2-21-1 Osawa, Mitaka, Tokyo 181-8588, Japan*
[9]*Department of Physics and Astronomy, University of Waterloo, Waterloo, Ontario, N2L 3G1, Canada*
[10]*Leiden Observatory, Leiden University, PO Box 9513, NL-2300 RA Leiden, the Netherlands*
[11]*Herschel Science Centre, European Space Astronomy Centre, ESA, Villanueva de la Cañada, E-28691 Madrid, Spain*
[12]*Instituto de Astrofisica, Facultad de Fisica, Pontificia Universidad Catolica de Chile, 306, Santiago 22, Chile*
[13]*Space Science Institute, 4750 Walnut Street, Suite 205, Boulder, CO 80301, USA*
[14]*Department of Physics, Durham University, South Road, Durham, DH1 3LE, UK*
[15]*Department of Astronomy and Astrophysics, 525 Davey Laboratory, The Pennsylvania State University, University Park, PA 16802, USA*
[16]*INAF-Osservatorio Astronomico di Bologna, Via Ranzani 1, I-40127 Bologna, Italy*
[17]*Dipartimento di Astronomia, Università di Bologna, Via Ranzani 1, I-40127 Bologna, Italy*
[18]*Center for Galaxy Evolution, Department of Physics and Astronomy, University of California, Irvine, 4129 Frederick Reines Hall Irvine, CA 92697, USA*

Downloaded from https://academic.oup.com/mnras/article/445/3/2725/1041622 by guest on 18 December 2021

[19]*NASA Herschel Science Center, Caltech 100-22, Pasadena, CA 91125, USA*
[20]*LAM, CNRS-UNiv Aix-Marseille, 38 rue F. Joliot-Curis, F-13013 Marseille, France*
[21]*Argelander-Institut für Astronomie, Universität Bonn, Auf dem Hügel 71, D-53121 Bonn, Germany*
[22]*The Observatoires of the Carnegie Institution of Science, 813 Santa Barbara Street, Pasadena, CA 91101, USA*
[23]*School of Physics and Astronomy, The Raymond and Beverly Sackler Faculty of Exact Sciences, Tel Aviv University, Tel Aviv 69978, Israel*
[24]*Department of Physics and Astronomy, University of Pittsburgh and PITT-PACC, 3941 O'Hara St., Pittsburgh, PA 15260, USA*

This paper has been typeset from a TEX/LATEX file prepared by the author.

Downloaded from https://academic.oup.com/mnras/article/445/3/2725/1041622 by guest on 18 December 2021